Biochimica et Biophysica Acta 1788 (2009) 425–441

Contents lists available at ScienceDirect

Biochimica et Biophysica Acta

journal homepage: www.elsevier.com/locate/bbamem

Fluorescent sterols monitor cell penetrating peptide Pep-1 mediated uptake and intracellular targeting of cargo protein in living cells

Anca D. Petrescu [b], Aude Vespa [b], Huan Huang [b], Avery L. McIntosh [b], Friedhelm Schroeder [b], Ann B. Kier [a,*]

[a] Department of Pathobiology, Texas A and M University, TVMC, College Station, TX 77843-4467, USA
[b] Department of Physiology and Pharmacology Texas A and M University, TVMC College Station, TX 77843-4467, USA

ARTICLE INFO

Article history:
Received 26 June 2008
Received in revised form 25 August 2008
Accepted 24 September 2008
Available online 17 October 2008

Keywords:
Acyl-CoA binding protein
Confocal microscopy
Dansyl-cholestanol
Dehydroergosterol
Endocytosis
Macropinocytosis
Multiphoton excitation

ABSTRACT

Although cell-penetrating peptides (CPP) facilitate endocytic uptake of proteins, little is known regarding the extent to which CPPs facilitate protein cargo exit from endocytic vesicles for targeting to other intracellular sites. Since the plasma membrane and less so intracellular membranes contain cholesterol, the fluorescent sterol analogues dansyl-cholestanol (DChol) and dehydroergosterol (DHE) were used to monitor the uptake and intracellular distribution of fluorescent-tagged acyl coenzyme A binding protein (ACBP) into COS-7 cells and rat hepatoma cells. Confocal microscopy colocalized DChol and Texas Red-ACBP (TR-ACBP) with markers for the major endocytosis pathways, especially fluorescent-labeled cholera toxin (marker of ganglioside GM1 in plasma membrane lipid rafts) and dextran (macropinocytosis marker), but less so with transferrin (clathrin-mediated endocytosis marker). These findings were confirmed by multiphoton laser scanning microscopy colocalization of TR-ACBP with DHE (naturally-fluorescent sterol) and by double immunofluorescence labeling of native endogenous ACBP. Serum greatly and Pep-1 further 2.4-fold facilitated uptake of TR-ACBP, but neither altered the relative proportion of TR-ACBP colocalized with membranes/organelles (nearly 80%) vs cytoplasm and/or nucleoplasm (20%). Interestingly, Pep-1 selectively increased TR-ACBP associated with mitochondria while concomitantly decreasing that in endoplasmic reticulum. In summary, fluorescent sterols (DChol, DHE) were useful markers for comparing the distributions of both transported and endogenous proteins. Pep-1 modestly enhanced the translocation and altered the intracellular targeting of exogenous-delivered (TR-ACBP) in living cells.

1. Introduction

The cell surface membrane functions as a barrier preventing passive entry of xenobiotics, proteins, antibodies, drugs, toxins, DNA, RNA, and living microorganisms. However, therapeutics increasingly requires delivery of biologically active macromolecule cargoes into cells (rev. in [1]. While microinjection or electroporation bypass the endocytosis/lysosomal degradative pathway to deliver active macromolecules into cells, these methods are invasive, exhibit low efficiency, poor specificity, and toxicity (rev. in [1–3]. Therefore, increasing interest has focused on the use of specialized cell penetrating peptides (CPP) to facilitate macromolecule (cargo) entry into cells (rev. [1,3–6]. CPPs evolved as small polypeptide regions of certain proteins enabling them to circumvent the plasma membrane barrier to gain entry into the cell and exert their biological effects.

The mechanism(s) whereby CPPs and CPP-mediated cargo are translocated through biological membranes is a very active, controversial area of investigation (rev. in [4,5]. CPP transduction and CPP-mediated cargo transduction through the cell surface membrane was originally thought to be non-saturable, dose-dependent, temperature-independent, and energy independent — thereby excluding endocytosis (rev. in [1,4–6]. However, subsequent investigations showed that some of the early conclusions were complicated by experimental artifacts (rev. in [1,7]. Instead many CPPs, especially those covalently attached to cargo proteins, are taken up and facilitate cargo uptake into living cells via one or more of the well-known endocytic routes including clathrin-coated vesicles, lipid rafts, caveolae, or macropinocytosis (rev. in [1,3–6,8–10]. Interestingly, it was recently reported that endocytosis inhibitors clearly reduced the Pep-1 (non-covalently attached to cargo protein) mediated translocation efficiency of fluorescent labeled β-galactosidase into HeLa cells but did not result in colocalization with endosomes, lysosomes, or caveosomes in fixed HeLa cells [11,12]. Taken together, these data suggest that non-covalently attached CPPs such as Pep-1 may facilitate both endocytic and non-endocytic uptake of cargo protein [2,12,13].

Despite the above advances, however, it is not clear whether the CPPs such as Pep-1 not only facilitate endocytic entry of non-

Abbreviations: ACBP, acyl coenzyme A binding protein; DChol, dansyl-cholestanol; DHE, dehydroergosterol; LUV, large unilamellar vesicles; CPP, cell penetrating peptide; CD, circular dichroism; LSCM, laser scanning confocal microscopy; MPLSM, multiphoton laser scanning microscopy

* Corresponding author. Tel.: +1 979 862 1509; fax: +1 979 862 9231.
E-mail address: akier@cvm.tamu.edu (A.B. Kier).

0005-2736/$ – see front matter © 2008 Elsevier B.V. All rights reserved.
doi:10.1016/j.bbamem.2008.09.015

covalently bound cargo protein but also enhance cargo protein exit from endocytic vesicles into the cytoplasm of cells. In fact, almost nothing is known about the proportion of CPP cargo that actually enters the cytoplasm. The fact that CPP mediated protein transduction does elicit functional responses in living cells clearly suggests that at least some of the translocated protein enters the cytoplasm for targeting cellular functions [7,8,14,15]. However, it is not known whether this represents a minority or a significant proportion of cargo protein exit from endocytic pathways, entry into cytoplasm, and correct redistribution to intracellular organelles in a manner similar to the respective endogenous protein (rev. in [1,3–6].

The current investigation was undertaken to develop the use of fluorescent sterols (DChol and DHE) as markers for exogenous protein translocation and association of both exogenous and endogenous protein with membranes and endocytosed plasma membrane vesicles. The fluorescent sterols were chosen as membrane markers because, with the exception of the inner mitochondrial membrane, all mammalian membranes contain significant amounts of cholesterol ranging from as much as 50% of total lipid (plasma membrane) to about 20% of total lipid (endoplasmic reticulum) (rev. in [16–20]. ACBP was chosen as a model cargo protein because of its small size (10 kDa), distribution throughout the cytoplasm, association with select organelles, and ability to pass through nuclear pores (too small to accommodate endocytic vesicles) into the nucleoplasm for interaction with nuclear receptors (rev. in [21,22]. The results showed that the fluorescent sterols (DChol, DHE) were useful markers comparing the distributions of both transported and endogenous proteins. While Pep-1 did not alter the relative proportions of membrane vs cytosol/nucleoplasm associated TR-ACBP, Pep-1 modestly enhanced the translocation and altered the intracellular targeting of exogenous-delivered (TR-ACBP) by shifting TR-ACBP distribution away from endoplasmic reticulum toward mitochondria.

2. Materials and methods

2.1. Materials

Pep-1 (Chariot™) was obtained from Active Motif (Rikensart, Belgium). Ni-CAM resin and protease inhibitor cocktail were purchased from Sigma, St-Louis, MO. BioGel P4 resin was from Bio-Rad (Hercules, CA). Two-well LabTek coverglasses, from VWR (Sugarland, TX). BCA protein assay kit was from Pierce Biotechnology Inc. (Rockford, IL). COS-7 cells were obtained from the American Type Culture Collection (Manassas, VA). 1-Palmitoyl-2-oleoyl-sn-glycero-3-phosphatidylcholine (POPC) was from Avanti Polar Lipids (Alabaster, AL). *Cis*-parinaric acid (naturally-fluorescent fatty acid) was obtained from Molecular Probes, Invitrogen (Eugene, OR). *Cis*-parinaroyl-CoA (natural-fluorescent fatty acyl CoA) was synthesized as described earlier [23]. Vital dye markers for plasma membrane and intracellular membrane organelles were obtained from Molecular Probes, Invitrogen (Eugene, OR) as follows: Alexa Fluor 488 (CT-488) and 594 (CT-594) cholera toxin subunit B (CT-B) conjugates (markers for ganglioside GM1 present in plasma membrane lipid rafts), Texas Red-dextran (marker for macropinocytosis), Texas Red-transferrin (marker for clathrin-coated pits and vesicles), LysoTracker Yellow-HCK123 (marker for lysosomes), ER-Tracker Green (i.e. glibenclamide BODIPY-FL) (marker for endoplasmic reticulum), NBD-C6-ceramide (marker for Golgi complex), MitoFluor Green (marker for mitochondria), and Hoechst 33342 (marker for nucleus). Texas Red–X succinimidyl ester was purchased from Molecular Probes (Invitrogen Life Technologies, Carlsbad, CA) while Cy5 labeling kit was from Amersham Biosciences Corp. (Piscataway, NJ). Antibodies to membrane organelle markers for fixed cells were purchased as follows: anti-cathepsin D antibody (Sigma Chemical Co., St. Louis, MO), anti-mitochondrial HSP70 antibody (Affinity Bioreagents, Inc., Golden, CO), and Texas Red- and FITC- anti-rabbit, anti-rat, anti-mouse IgGs (Molecular Probes, Invitrogen, Eugene, OR). Concanavalin-FITC (ER marker of fixed cells) and wheat germ agglutinin-FITC (Golgi marker of fixed cells) were obtained from Sigma (St. Louis, MO). Dulbecco modified Eagle's medium (DMEM), fetal bovine serum (FBS), phosphate saline buffer (PBS) and Hank's solutions were from Invitrogen (Carlsbad, CA).

2.2. Expression and purification of recombinant of acyl CoA binding protein (ACBP)

C-terminal histidine tagged recombinant mouse ACBP was expressed in *E. coli* BL21 cells from a pET21b vector under IPTG induction, and purified by affinity chromatography on Ni-CAM resin as described [24]. Protein concentration was determined in each elution fraction by BCA assay. Purity of his-ACBP was assessed by SDS-PAGE in 14% acrylamide gels according to a Bio-Rad procedure [25] followed by Coomassie blue staining. His-ACBP appeared as a single band at the expected molecular weight near 11 kDa. Western blotting of his-ACBP was performed to confirm identity by using locally-produced rabbit polyclonal antiserum raised against native rat liver ACBP, as previously described [22].

2.3. Labeling of recombinant ACBP protein with fluorescent dyes: Texas Red and Cy5

The surface of ACBP exhibits 7 exposed amino acid residues with free amino groups [26]. Therefore, His-ACBP was covalently labeled with the fluorescent tag Texas Red by use of a Texas Red-X succinimidyl ester labeling kit from Molecular Probes/Invitrogen (Eugene, OR) or by use of a Cy5 labeling kit from Amersham Biosciences Corp. (Piscataway, NJ) according to the manufacturers' instructions. To minimize the number of dye/ACBP protein molecule, generally 0.5 mg his-ACBP was incubated with dye/DMSO in a 1:5 protein/dye molar ratio, in phosphate buffer saline (PBS), pH 8.5, with stirring for 1 h at room temperature. After removing possible aggregates by a brief centrifugation at 20,000 ×*g* , the dye/protein conjugate was isolated from unreacted dye by gel-exclusion chromatography on BioGel P4 resin. Qualitative determination of final dye-labeled ACBP products were performed by SDS-PAGE and Western blotting. The molecular size of dye-his-ACBP conjugates and dye-to-protein molar ratios were determined by matrix assisted laser desorption mass spectrometry (MALDI) performed at the Texas A&M University Mass Spectrometry Laboratory.

2.4. Circular dichroism (CD) analysis of dye-labeled ACBP as compared to unlabeled ACBP recombinant protein

To assure that covalent labeling of his-ACBP with fluorescent tags (TR, Cy5) did not alter his-ACBP structure, far ultraviolet (UV) circular dichroic (CD) spectra of Texas Red- and Cy5-labeled, recombinant mouse ACBP and unlabeled-ACBP were measured in 30 mM phosphate buffer, pH 7.4 using a J-710 spectropolarimeter (Jasco, Baltimore, MD) and 1 mm cuvette as described earlier [24]. Spectra were recorded from 260 to 190 nm at 50 nm/min, with integration time of 1 s and a bandwidth of 2 nm. An average of 10 scans were run for each CD profile. Percentage composition of secondary structures was calculated by using CDPRO software as described [27].

2.5. Fluorescent ligand binding assay of dye-labeled ACBP

To assure that covalent labeling of his-ACBP with fluorescent tags (TR, Cy5) did not alter his-ACBP function, the affinity of dye-labeled ACBP for a long chain fatty acyl CoA ligand was determined. *Cis*-parinaroyl-CoA is the CoA thioester of a naturally-occurring fluorescent fatty acid, i.e. *cis*-parinaric acid [23,24,28]. *Cis*-parinaroyl-CoA binding was determined by measuring: i) the increase in ligand fluorescence intensity at 420 nm with excitation at 320 nm, upon

binding to protein; ii) quenching in ACBP tyrosine and tryptophan fluorescence intensity at 340 nm upon excitation at 280 nm upon ligand binding to protein. Tyr and Trp fluorescence emission overlaps with cis-parinaroyl-CoA emission — thereby making this an effective donor/acceptor pair for fluorescence resonance energy transfer when the two are in close proximity, i.e. a few angstroms. Usually, 30 nM dye-labeled ACBP was titrated with 2.5–300 nM *cis*-parinaroyl CoA and fluorescence emission spectra were recorded: i) from 380–440 nm upon excitation of ligand at 320 nm; ii) from 290–400 nm upon excitation at 280 nm. Fluorescence emission spectra were obtained using a PC1 photon counting fluorimeter (ISS Inc. Urbana, IL). Maximum fluorescence intensities of *cis*-parinaroyl-CoA at 420 nm at each titration point were plotted versus ligand concentrations after subtraction of corresponding control values in which ACBP was not present. In quenching experiments, F_0–F, the amount of quenching at each titration point was plotted against the corresponding ligand concentration. B_{max} and K_d values were obtained by curve fitting, using SigmaPlot software (SYSTAT, San Jose, CA), and fitting to the one site binding saturation option of the program as described earlier for untagged fatty acyl CoA binding proteins.

2.6. Fluorescent sterol synthesis and incorporation into large unilamellar vesicles (LUV): dansyl-cholestanol (DChol) and dehydroergosterol (DHE)

Dansyl-cholesterol was synthesized as previously described [29]. Dehydroergosterol was prepared according to a modified protocol of an earlier procedure as described earlier [30–32]. DChol and DHE were incorporated into model membrane vesicles (i.e. LUV, large unilamellar vesicles) for incorporation into cells basically as described earlier for DHE [32]. LUVs consisting of 35% DChol or DHE and 65% 1-palmitoyl-2-oleoyl-sn-glycero-3-phosphatidylcholine (POPC) molar fractions were prepared as described [32]. Briefly, DChol/DHE and POPC dissolved in 95% ethanol were mixed and dried under nitrogen flow to produce a thin film which was dehydrated under vacuum overnight and dissolved in phosphate buffer saline (PBS) at 37 °C. The aqueous solution of DChol/DHE and POPC was then subjected to 5 cycles of freezing at −70 °C and thawing at 37 °C, and vigorous vortexing at each cycle. The resultant multilamellar dispersion was filtered through a 0.2 μm membrane (Millipore, Bedford, MA) and extruded by the use of an Avanti Mini-Extruder with a 0.1 μm polycarbonate membrane (Whatman). This stock solution of LUVs was diluted to 20 μg DChol or DHE/ml of cell culture medium.

2.7. Cell culture

For incorporation of fluorescent-tagged ACBP as well as fluorescent sterols for real time imaging by laser scanning confocal microscopy, COS-7 cells were seeded in 2-well LabTek chamber glasses and cultured in Dulbeco modified Eagle's medium (DMEM) containing 10% fetal bovine serum (FBS) under 5% CO2, at 37 °C, until 90% confluence as described [22].

2.8. Incorporation of DChol and DHE into cultured cells

Two different vehicles were used to deliver fluorescent sterols to COS-7 cells, namely fetal bovine serum (10% in DMEM) and LUV described above — both providing 20 μg sterol per ml of culture medium. When serum was utilized as DChol vehicle, COS-7 cells were seeded in LabTek chamber glasses and grown in 10% fetal bovine serum (FBS)-containing DMEM. At 80% confluence, the cells were washed with phosphate buffer saline (PBS) three times, shortly and incubated with serum-free DMEM culture medium for 30 min at 5% CO_2, 37 °C. Afterwards, the serum-free DMEM was replaced with 10% FBS/DMEM in which DChol and either an organelle fluorescent marker or fluorescent-labeled ACBP were added at the same time with DChol. The latter (DChol) was added from a 20 mg/ml ethanol stock solution to a final concentration of 20 μg/ml in the FBS/DMEM culture medium. Alternately DHE was added in the form of LUVs prepared as described above. COS-7 cells were first cultured in 10% FBS/DMEM medium, for 1 day at 5% CO2 and 37 °C; the cells were then supplemented with DChol/DHE-POPC LUV solution at a final concentration of 20 μg/ml sterol in FBS/DMEM; cells were grown for two more days under the same conditions. Before confocal microscopy imaging, cells were processed for the uptake of fluorescent ACBP in the absence or presence of Pep-1 (as described below).

2.9. Pep-1-mediated uptake of fluorescent labeled ACBP into COS-7 cells

COS-7 cells were grown in 2-well LabTek chamber glasses in 10% FBS-containing DMEM to 80% confluence. Texas Red- or Cy5-labeled ACBP (0.5 μg/ml) was first mixed with Pep-1 (0.5 μg/ml) for 30 min at room temperature in order to form protein-peptide complex, then added to cells in serum-depleted DMEM. After incubation for 30 min at 37 °C, the ACBP/Pep-1 complex was washed from cells with phosphate buffer saline and replaced with 10% FBS-DMEM. In time-course experiments, laser scanning confocal microscopy (LSCM) was performed after the addition of serum-DMEM at various time points from 5 min to several hours as indicated in Results section. In experiments where imaging was done at time points equal or longer than 30 min, the staining of cell nuclei with vital Hoechst DNA dye (at a final concentration of 1 μg/ml) was applied; the nuclear marker was added at 30 min before taking the confocal microscopy images.

2.10. Distribution of DChol and DHE with endocytic markers in plasma membranes of living cells

Uptake of DChol and DHE into endocytic regions of plasma membranes was determined by laser scanning confocal microscopy (LSCM) imaging and multiphoton laser scanning microscopy (MPLSM), respectively. DChol and DHE at the plasma membrane were colocalized with known lipid raft and endocytosis markers such as: i) cholera toxin subunit B, marker for GM1 in lipid rafts; ii) transferrin, marker for clathrin dependent endocytosis; iii) 10 kDa dextran, marker of macropinocytosis. Briefly, cells were cultured in DMEM supplemented with 10% serum (FBS) for 2 days, until they reached 80% confluence. Just before confocal microscopy imaging, cells were washed and incubated with cold PBS on ice (at 4 °C) for 20 min. Simultaneously, a cold solution of DMEM supplemented with 10% FBS, 20 μM DChol and the raft or endocytosis fluorescent marker, was prepared and cooled on ice. The concentrations of markers were: i) 5 μg/ml for cholera toxin labeled with Alexa Fluor 488 (CT-488) or Alexa Fluor 594 (CT-594); ii) 100 μg/ml Texas Red-transferrin; iii) 100 μg/ml Texas Red-dextran (10 kDa). Cells were incubated with this mix of FBS, DMEM, DChol, and endocytic marker for 5 more minutes on ice, and quickly processed for LSCM of DChol and markers (see below) or multiphoton laser scanning microscopy (MPLSM) for DHE and markers (see below) to minimize the redistribution and internalization of labels as reported previously by our laboratory [32].

2.11. Distribution of fluorescent sterols and dye-labeled ACBP with endocytic and organelle markers

In order to assess colocalization of fluorescent-tagged ACBP with fluorescent sterols (DChol, DHE) and vital dye labeled membranes/organelles, the fluorescent sterols and fluorescent-tagged ACBP were incorporated into COS-7 cells as described above, imaged by LSCM (DChol) or MPLSM (DHE), and colocalized in living cells as described earlier [32]. Vital dyes used were cholera toxin B-Alexa Fluor 488 (CT-488) conjugate (marker for plasma membrane lipid rafts), Texas Red-dextran (marker for macropinocytic vesicles), Texas Red-transferrin (marker for clathrin coated pits and vesicles), LysoTracker Yellow-

HCK123 (marker for lysosomes); ER-Tracker Green (glibenclamide BODIPY-FL, marker for endoplasmic reticulum); NBD-C6-ceramide (marker for Golgi); MitoFluor Green (marker for mitochondria); and Hoechst 33342 (marker for nucleus). All markers were used as recommended by manufacturer. Dye-labeled ACBP (TR or Cy5) colocalization with fluorescent sterols or vital dye fluorescent organelle markers was also performed after incorporating dye-labeled ACBP in the presence of Pep-1. Briefly, 2 h after incubation with serum-supplemented DMEM at 37 °C post TR-ACBP ± Pep-1 treatment, cells were first labeled with 1 μg/ml Hoechst 33342 nuclear dye in serum/DMEM at 37 °C for 30 min, and then with LysoTracker Yellow (1 μM in serum/DMEM at 37 °C for 30 min), ER-Tracker Green (1 μM in Hank's solution with Ca^{2+} and Mg^{2+}, for 15 min at 37 °C) or MitoFluor Green (100 nM in serum/DMEM at 37 °C for 30 min). Labeling of Golgi complex with NBD-C6-ceramide/albumin was also performed after pre-treatment of cells with TR-ACBP ± Pep-1 and nuclear marker, by incubating cells with 5 μM NBD-C6-ceramide/albumin in Hank's solution for 30 min at 37 °C as recommended by manufacturer.

2.12. Real-time imaging of fluorescent sterols, dye-labeled ACBP, and markers in living cells

For all studies involving imaging of DChol, LSCM was performed by using a fluorescence confocal imaging system (MRC-1024, Bio-Rad, Hercules, CA) consisting of an inverted microscope (Axiovert 135, Zeiss, New York, NY) equipped with three independent low-noise photomultiplier tube (PMT) channels. The excitation light (488 nm, 568 nm and 647 nm) from a 15 mW krypton-argon laser was delivered to sample through a 63X oil immersion objective (Zeiss Plan-Fluor, New York NY), with numerical aperture of 1.4, while the emission fluorescence light was detected in photomultiplier tubes (PMTs) by using emission filters 585 LP in PMT1, 540/30 in PMT2, and 680/32 in PMT3. Since DHE is a UV excitable fluorescent sterol (excited in the range 300–324 nm), but is readily bleached by direct UV excitation, DHE was instead excited by three-photon excitation at 900 nm (conditions under which DHE is much more stable, i.e. undergoes very little photobleaching) and DHE fluorescence emission was imaged by MPLSM using the MRC-1024 multiphoton configuration and external detectors as described earlier [32,33]. Images were acquired and analyzed with LaserSharp (Bio-Rad) and MetaMorph (Advanced Scientific Imaging) [22,32,33].

2.13. Immunofluorescence LSCM of ACBP localization in fixed cells

T-**7** rat hepatoma cells (received from Dr. Charles Baum, University of Chicago, Chicago, IL) expressing high amounts of endogenous ACBP [22] were grown in 2-well LabTek chamber slides in high-glucose DMEM with 10% FBS, and fixed with 4% glutaraldehyde at 37 °C for 30 min, residual aldehyde was quenched with ammonium chloride, and then nonspecific antibody binding was blocked with 5% FBS in Hank's solution. Primary antibodies raised against ACBP were produced locally in rabbit or rat [22,24,34], while all other primary and secondary antibodies used as membrane/organelle markers were commercially purchased as stated under Materials. Double immunolabeling LSCM to colocalize ACBP with membrane organelle markers was performed similarly as described earlier for ACBP and specific organelle markers including anti-cathepsin D antibody (lysosomes), anti-mitochondrial HSP70 antibody (mitochondria), concanavalin-FITC (marker for endoplasmic reticulum) and wheat germ agglutinin-FITC (marker for Golgi system) [22]. Secondary antibodies were Texas Red- or FITC-labeled antirabbit, antirat, anti-mouse IgGs. Cells that had been fixed and blocked for nonspecific binding were incubated with 5 μg/ml primary antibody in 2% FBS/Hank's solution for 1 h at room temperature followed by three washings with Hank's solution and 1 h incubation with 5 μg/ml secondary antibody at room temperature. After washing away the secondary antibody with Hank's solution, cells were prepared for confocal microscopy by the use of anti-fading kit SlowFade from Molecular Probes (Invitrogen, Eugene, OR).

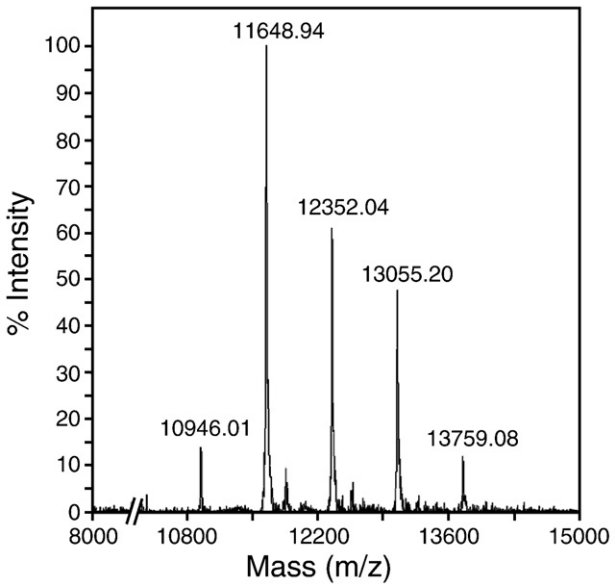

Fig. 1. Mass spectrometry analysis of Texas Red-labeled ACBP. Distinctive peaks of MS detection intensity can be seen, corresponding to: unlabeled ACBP (MW 10946); TR dye-ACBP, molar ratio 1:1 (MW 11649); TR-ACBP, molar ratio 2:1 (MW 12352); TR-ACBP, molar ratio 3:1 (MW 13055), and 4:1 (MW 13759).

3. Results

3.1. Structural and functional characterization of Texas Red-labeled ACBP (TR-ACBP)

TR-ACBP was analyzed by mass spectrometry to determine the number of covalently attached TR molecules per molecule of protein. The small intensity peak detected at 10946.01 Da (17% of total intensity) corresponded to unlabeled his-ACBP (Fig. 1). Additional mass spectral peaks at 11648.94, 12352.04, and 13055.20 Da corresponded to his-ACBP labeled with one (43% of total intensity), two (26% of total intensity), or three (20% of total intensity) TR/his-ACBP, respectively. Thus, the TR labeled nearly 90% of ACBP and TR-ACBP with a 1:1 dye-to-protein molar ratio as the highest fraction.

To examine if TR labeling altered ACBP structure, samples were examined by SDS-PAGE (detect cross-linking), Western blotting (detect altered antibody specificity), and circular dichroism (CD, detect altered secondary structure). TR labeling did not result in the formation of intermolecular cross-links between his-ACBP protein molecules as shown by SDS-PAGE which detected a single band (Fig. 2A), consistent with the molecular weight of monomeric protein determined by mass spectrometry (Fig. 1). Western blotting demonstrated that ACBP antigenic specificity was maintained after labeling with TR (Fig. 2B). CD spectra of TR-ACBP and ACBP were similar, indicating that TR labeling did not alter ACBP molar ellipticity or secondary structure (Fig. 2C).

To determine if TR labeling altered his-ACBP ligand interaction, binding of *cis*-parinaroyl-CoA was examined (Fig. 2D). Quantitative analysis of multiple saturation binding curves yielded a K_d value of 40.8 + 9.8 nM for TR-ACBP (Fig. 2D). Saturation binding was confirmed by quenching in ACBP Tyr/Trp fluorescence upon *cis*-parinaroyl-CoA binding which yielded a K_d of 21.3 + 5.2 nM for TR-ACBP (Fig. 2E). Previous analysis of *cis*-parinaroyl-CoA binding by unlabeled ACBP using the same binding assays demonstrated K_d's near 5 nM, [24]. Although TR labeling decreased his-ACBP's ligand binding affinity

somewhat, nevertheless the affinity of TR-ACBP K_d for *cis*-parinaroyl-CoA was still high, i.e. low nM range. Since the intracellular, cytosolic long chain acyl-CoA concentration in COS-7 cells in culture is in the μM range, this suggested that TR-ACBP maintained its function as an effective fatty acyl CoA binding protein in the physiological range of fatty acyl CoA concentrations in the cytosol [35,36].

Taken together the above data showed that Texas Red labeling did not induce formation of protein-protein dimers, alter antigenic responsiveness, or alter ACBP secondary structure and minimally altered ACBP function in ligand binding.

3.2. Incorporation of dansyl-cholesterol (DChol) from serum into the plasma membrane of live COS-7 cells

In order to resolve whether basal or Pep-1 mediated translocation of exogenous proteins such as TR-ACBP results in exit of endocytosed TR-ACBP into the cytoplasm/nucleoplasm, it was important to develop probe molecules that reported on plasma membranes, endocytic membranes, membrane domains, and membranous organelles. Since all cellular membranes (except the inner mitochondrial membrane) as well as plasma membrane cholesterol-rich and –poor microdomains contain cholesterol, the possibility that fluorescent sterols dansyl-cholesterol (DChol) and dehydroergosterol (DHE) could be used as markers reporting on these membranes, domains, and membrane organelles was determined. To examine DChol incorporation into plasma membrane cholesterol-rich microdomains in the absence significant endocytic uptake, COS-7 cells were incubated with DChol in the presence of serum and DChol at 4 °C (temperature at which energy-dependent endocytic mechanisms are inhibited). Immediately thereafter, the co-distribution of serum-delivered DChol with cholera toxin subunit B labeled with Alexa Fluor 488 or 594 (CT-488 or CT-594) was then determined by simultaneously acquiring LSCM images of DChol (green) and Alexa Fluor CT dyes (red) through separate photomultipliers. Superposition of Dchol (green) and cholera toxin (red) images when cholera toxin was labeled with CT488 (Fig. 3A) and 594 (Fig. 3C) dyes, respectively, revealed that incubation at 4 °C resulted in most of the DChol and Alexa Fluor-labeled cholera toxin B appearing at the plasma membrane as highly colocalized (yellow/orange pixels). Some DChol (green) was diffusely distributed in the cytoplasm, and only very little of the Alexa Fluor CT probes, especially CT488, appeared inside the cells. To confirm this pattern of distribution, display of only the colocalized pixels (yellow) of DChol with CT-488 (Fig. 3B) and CT-594 (Fig. 3D), respectively, indicated high colocalization at the plasma membrane, but only rarely detected within the cell. The colocalization pattern at the plasma membrane reflected mostly high intensity clusters of colocalized DChol/Alexa Fluor CT pixels interspersed with small less intense areas of relatively low colocalization (Fig. 3B and D), low DChol (Fig. 3A and C, green pixels), and/or low Alexa Fluor CT (Fig. 3A and C, red pixels). Quantitative analysis of DChol colocalization in multiple cells labeled

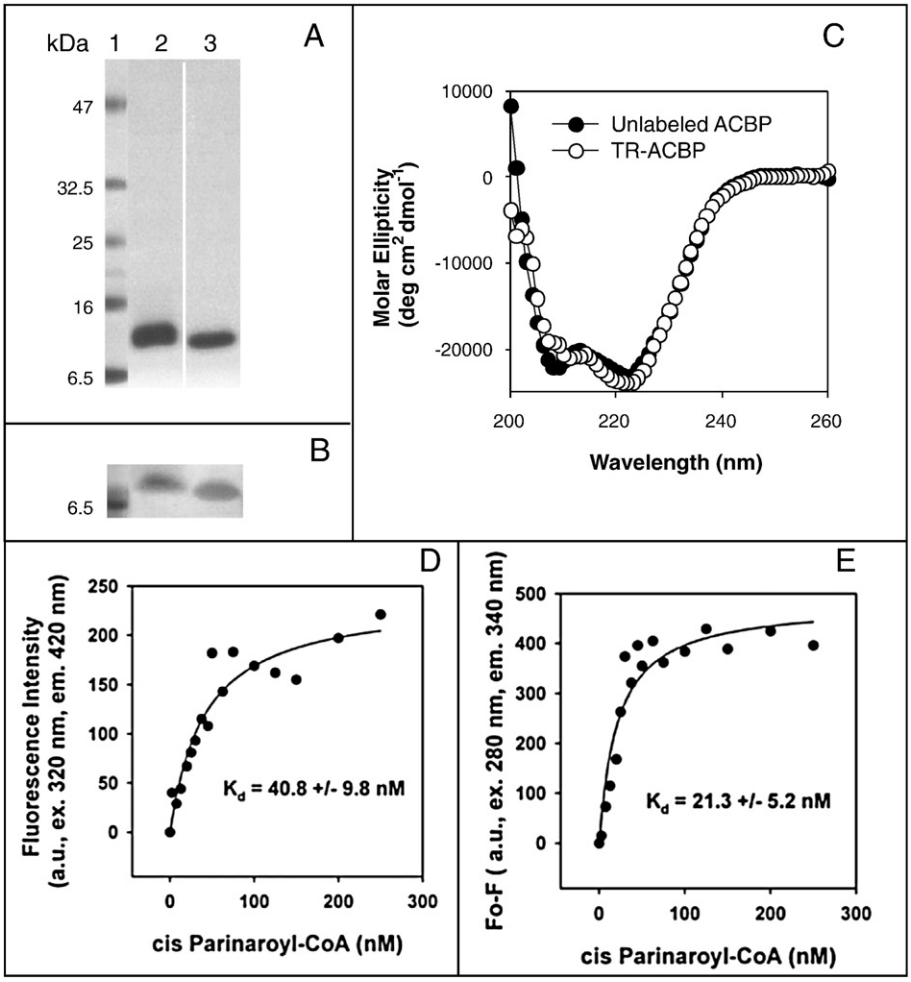

Fig. 2. Structural and functional characterization of Texas Red-labeled ACBP (TR-ACBP). (A) SDS-PAGE of TR-ACBP (lane 2), unlabeled ACBP (lane 3); lane 1 shows molecular size markers. (B) Western blot of TR-ACBP (lane 2) and unlabeled ACBP (lane 3); lane 1 shows molecular size marker. (C) Circular dichroic (CD) spectrum of TR-ACBP (solid circles) versus unlabeled ACBP (open circles). (D) Ligand (*cis*-parinaroyl-CoA) binding curve of TR-ACBP as determined by increase in ligand fluorescence intensity at 420 nm with excitation at 320 nm, upon binding to protein. (F) Binding curve as determined by measuring quenching of TR-ACBP intrinsic (Tyr/Trp) fluorescence at 340 nm with excitation at 280 nm, upon titration with cis-parinaroyl-CoA.

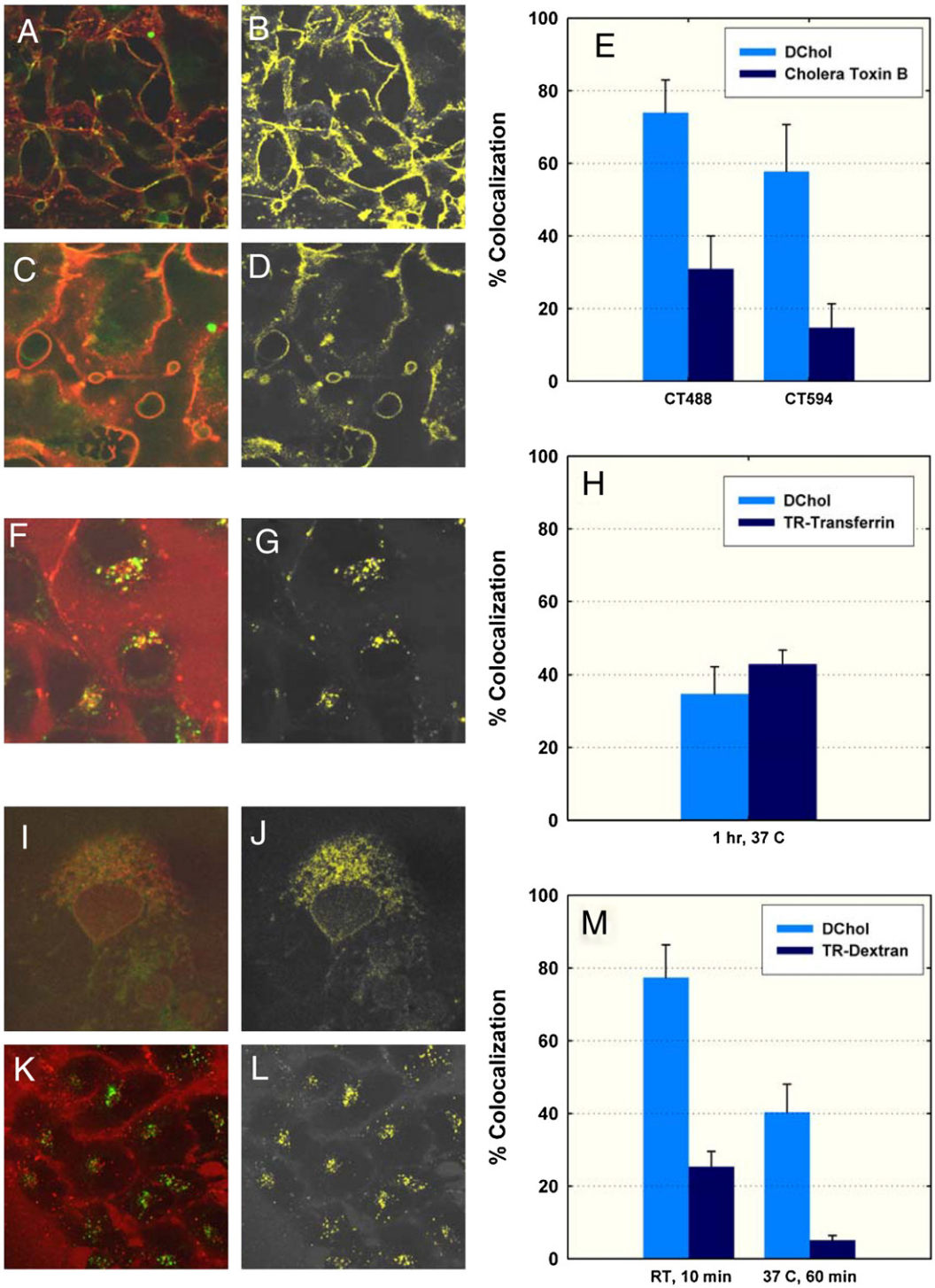

Fig. 3. Colocalization of dansyl-cholesterol (DChol) with lipid raft and endocytosis markers in live COS-7 cells. (A, C) Overlay images of Dchol (green) and cholera toxin B (CT) labeled with Alexa Fluor(AF)-488 (A) or AF-594 (C). (B, D) Colocalized pixels from A and C, respectively were selected (shown in yellow). (E) Bar graph of Dchol colocalization with CT488 or CT594 within first 5 min at room temperature after coincubation of DChol and cholera toxin with COS-7 cells at 4 °C for 20 min. (F-H) Colocalization of Dchol with TR-transferrin: (F) Overlay of DChol (green) and TR-transferrin (red) fluorescence images; (G) Colocalized pixels from F were selected (shown in yellow); (H) Bar graph of DChol colocalization with TR-transferrin after 1 h incubation with cells at 37 °C. (I–M) Colocalization analysis for DChol with TR-dextran: (I, K) Overlay of Dchol (green) and TR-dextran (red) fluorescence images at 10 min, RT and 1 h, 37 °C incubation of cells with fluorescent markers, respectively; J, L, Colocalized pixels from I, K were selected (shown in yellow); (M) Bar graph of DChol colocalization with TR-dextran at 10 min, RT and 1 h, 37 °C.

with CT-488 or CT-594 at 4 °C for 20 min showed that 75% and 58% of DChol was found to be colocalized with CT-488 (Fig. 3E) and CT-594 (Fig. 3E), respectively. Thus, at low temperature (inhibits energy-driven endocytosis by vesicular mechanisms) most DChol was colocalized with cholera toxin-labeled cholesterol-rich microdomains at the plasma membrane, while 25–42% of DChol was not colocalized with Alexa Fluor-CT but resided in other regions of the plasma membrane or with some localized within the cells.

These data suggested that: i) DChol uptake via GM1 containing cholesterol-rich microdomains mediated endocytosis into COS-7 cells

was largely inhibited at 4 °C; ii) about 58–75% of DChol was associated with GM1-containing plasma membrane cholesterol-rich microdomains at 4 °C. Thus, serum-delivered DChol incubated at 4 °C with COS-7 cells appeared most highly colocalized with the GM1-marker cholera toxin subunit B at the plasma membrane cholesterol-rich microdomains.

3.3. Uptake of serum-delivered dansyl-cholesterol (DChol) by endocytic pathways in live COS-7 cells: clathrin-mediated pathway and macropinocytosis

To further investigate if DChol also enters the COS7 clathrin coated vesicle-mediated endocytosis pathway (via LDL receptors located within plasma membrane clathrin- domains), cells were coincubated with DChol and Texas-Red-labeled transferrin (TR-transferrin, a marker for clathrin- mediated endocytosis) in the presence of serum as DChol vehicle, at 4 °C or at permissive temperature, i.e. 37 °C. Coincubation of cells with DChol and TR-transferrin at 4 °C resulted in most of the TR-transferrin outside the cells with no detectable uptake of it into the cells (data not shown). Subsequent additional incubation for up to 1 h at 37 °C resulted in DChol and TR-transferrin detectable inside the cells where DChol was distributed diffusely in the cytosol and in punctuate vesicles that did not overlap with TR-transferrin vesicles (not shown). However, after 1 hour incubation of cells at 37 °C the TR-transferrin significantly colocalized with DChol inside the cells as shown by overlay of the simultaneously acquired DChol (green) and TR-transferrin (red) images (Fig. 3F). Display of only colocalized pixels (yellow) demonstrated that DChol which colocalized with TR-transferrin was distributed mostly inside cells in vesicular structures, but also in vesicles near the plasma membrane (Fig. 3G). Quantitative estimation of DChol/TR-transferrin colocalization in multiple cells indicated that 33% of DChol taken up into the cells was codistributed with TR-transferrin inside cells within vesicular structures after 1 h incubation of cells at 37 °C. Conversely, 42% of TR-transferrin was colocalized with DChol inside the cells—suggesting that incubation with DChol /serum had saturated the clathrin mediated pathway.

To determine if DChol also entered the macropinocytosis pathway of COS7 cells, cells were coincubated with DChol - in the presence of serum- and Texas Red-dextran (marker of fluid-phase endocytosis or macropinocytosis) at 4 °C for 20 min followed by additional coincubation at 24 °C for 10 min or 37 °C for 1 h. When cells were imaged after DChol /serum/ TR-dextran incubation at 24 °C for 10 min, overlay of simultaneously acquired images of DChol (green) and TR-dextran (red) showed a large number of yellow/orange punctuate structures indicating DChol/TR-dextran colocalization as well as additional DChol (green) in separate vesicular structures (Fig. 3I). Display of only the selected colocalized pixels (yellow) showed a bright punctuate distribution of colocalized pixels throughout the cell,

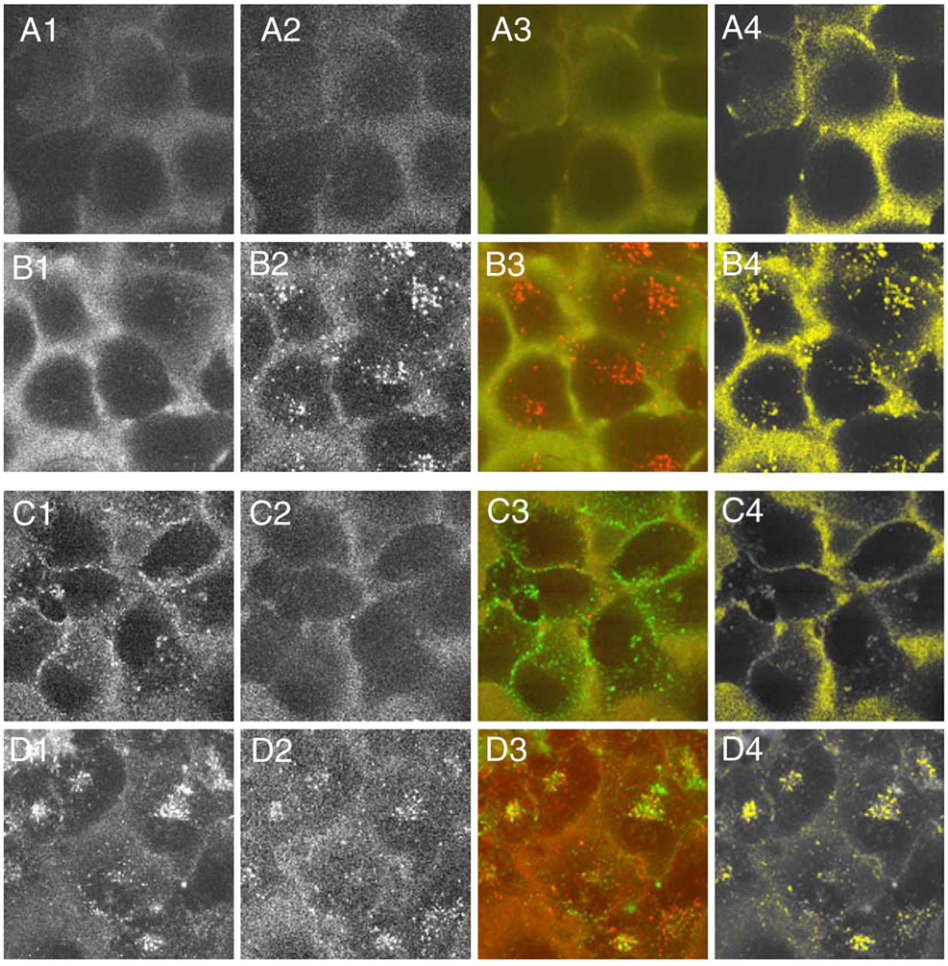

Fig. 4. Colocalization of Texas Red-labeled ACBP with endocytosis markers in live COS-7 cells. A mix of TR-ACBP and either Alexa Fluor 488-dextran or Alexa Fluor 488-transferrin was incubated with cells at 4 °C for 20 min as described under Materials and methods. (A1, A2) Images of Alexa488-dextran and TR-ACBP, respectively, in cells at a short time (5–10 min) after incubation at 4 °C. (A3) Overlay of TR-ACBP (red) and Alexa488-dextran (green) images. (A4) Colocalized red and green pixels in A3 were selected and are shown in yellow. (B1–B4) same as in A1-A4 but when images were taken after 60 min incubation of COS-7 cells with TR-ACBP and Alexa488-dextran at 37 °C. (C1, C2) Images of Alexa488-transferrin and TR-ACBP, respectively, in COS-7 cells after 10 min at RT post 4 °C incubation. (C3) Overlay of TR-ACBP (red) and Alexa488-transferrin (green) images. (C4) Colocalized red and green pixels in *C3* were selected and are shown in yellow. (D1–D4) same as in C1–C4 but after 60 min incubation of cells with TR-ACBP and Alexa488-transferrin at 37 °C.

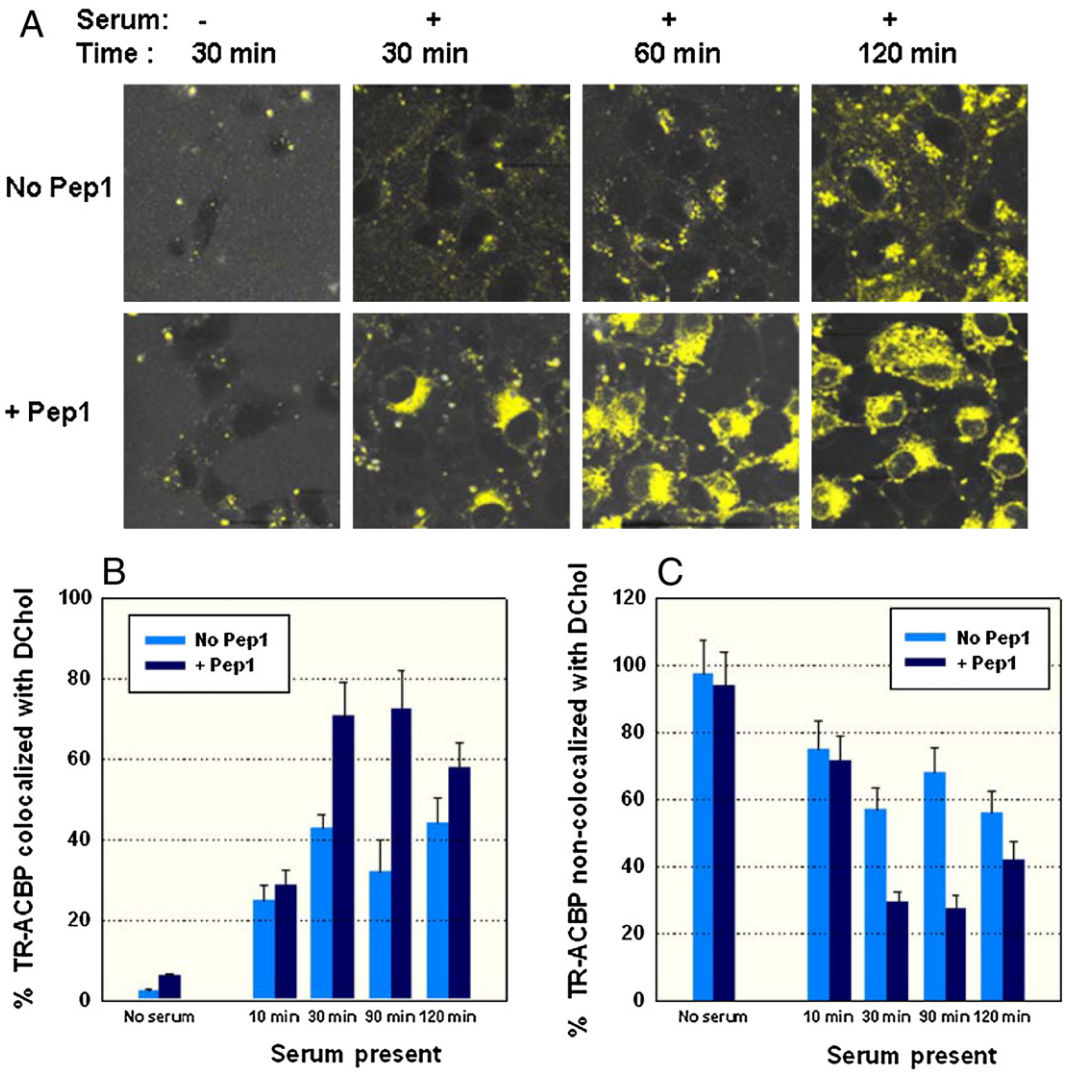

Fig. 5. DChol/TR-ACBP confocal colocalization monitored for TR-ACBP uptake into live COS-7 cells labeled with DChol/serum. (A) Colocalized pixels from TR-ACBP/Dchol overlay images (collected by LSCM with excitation of Texas Red and dansyl at 568 nm and 408 nm respectively, and emission filters HQ598/40 and 540/30 respectively); images were taken at time points as indicated from 30 min up to 2 h of chase after pulse, before and after serum addition. (B) Bar plot of percent TR-ACBP colocalized with DChol in the absence (blue) or presence (black) of Pep1, versus time. (C) Bar plot of percent TR-ACBP which was not associated with DChol versus time, in the absence (blue) or presence (black) of Pep1.

consistent with appearance of many small vesicles (Fig. 3J). This pattern was much more extensive and intense than that observed with TR-transferrin colocalization, even at longer time (Fig. 3J vs 3G). Quantitative analysis showed that 78% of DChol was colocalized with TR-dextran under these conditions (Fig. 3M). DChol was colocalized with TR-dextran nearly 3-fold more than TR-dextran colocalized with DChol — suggesting that incubation with serum-delivered DChol did not saturate the macropinocytosis pathway. In addition, the 78% colocalization of DChol with TR-dextran taken up by macropinocytosis was two fold higher than through the clathrin-mediated endocytosis (36% colocalization). It should be noted, however, that when cells were incubated with DChol/serum/ TR-dextran at 37 °C for 1 h, the overlay of simultaneously acquired images of DChol (green) and TR-dextran (red) showed much of the TR-dextran had recycled to the cell surface and was excreted back into the medium (red) (Fig. 3K). However, some TR-dextran remained within the cells colocalized with DChol in large perinuclear yellow/orange structures (Fig. 3K). Display of only the selected colocalized pixels (yellow) exhibited a bright punctuate codistribution only in the larger perinuclear areas (Fig. 3L). Quantitative analysis demonstrated that only 40% of DChol was colocalized with TR-dextran under these conditions (Fig. 3M). This suggested recycling and excretion of most of TR-dextran to leave fewer punctuate DChol/TR-dextran containing vesicles, consistent with the known pattern of fluid-phase macropinocytic uptake of large particles such as TR-dextran.

In summary, i) at 4 °C very little serum DChol delivered to plasma membranes was internalized, ii) at short time of incubation at 24 °C, DChol appeared highly colocalized with the macropinocytosis probe TR-dextran inside cells; iii) after 1 h incubation at 37 °C, DChol was equally distributed with TR-transferrin and TR-dextran. Thus, DChol was taken up from serum into cells by endocytic pathways involving not only plasma membrane cholesterol-rich microdomains (GM1, macropinocytosis) but also cholesterol-poor microdomain (clathrin-mediated endocytosis) pathways.

3.4. Uptake of Texas Red-Acyl CoA Binding Protein (TR-ACBP) by live COS-7 cells

To determine if TR-ACBP is internalized by clathrin-dependent endocytosis or macropinocytosis, COS-7 cells were cooled at 4 °C and treated with ice-cold medium containing serum, TR-ACBP and either Alexa Fluor 488-transferrin (marker for clathrin mediated endocytosis

pathway) or Alexa Fluor 488-dextran (marker for macropinocytosis pathway) followed by incubation at 37 °C for 10, 30, 60, or 120 min, and LSCM.

After short incubation times (e.g. 10–30 min), the Alexa488-dextran (macropinocytosis marker) (Fig. 4A1) was distributed not only at the cell surface but also taken up inside the cells as very small punctuate vesicles throughout the cell interior except for nuclei which appeared dark. Likewise, after short incubation times (e.g. 10–30 min) the TR-ACBP (Fig. 4A2) was taken up and distributed within cells as very small punctuate vesicles as well as throughout the cell interior and little in nuclei. At longer incubation time (2 h) more of the Alexa488-dextran (Fig. 4B1) and TR-ACBP (Fig. 4B2) were taken up into the cell interior and TR-ACBP appeared increasingly as higher intensity, larger punctuate vesicular structures became more prominent within the cell cytoplasm and near nuclei. Superposition of the images (Fig. 4A3), and even more so display of only colocalized pixels (Fig. 4A4), showed at short incubation time (10–30 min) the TR-ACBP was extensively colocalized with the macropinocytosis marker in very small punctuate vesicular structures distributed throughout the cytoplasm. At longer incubation times (1–2 h), superposition (Fig. 4B3) and display of only colocalized pixels (Fig. 4B4) showed even more intensity of colocalized TR-ACBP with Alexa488 dextran in the cell interior as well as some very bright punctuate regions near the nuclei.

With regards to the clathrin mediated endocytic pathway, after short incubation times (e.g. 10–30 min), the Alexa488-transferrin (clathrin mediated endocytosis marker) (Fig. 4C1) was distributed as many bright, larger punctuate vesicles, especially near the plasma

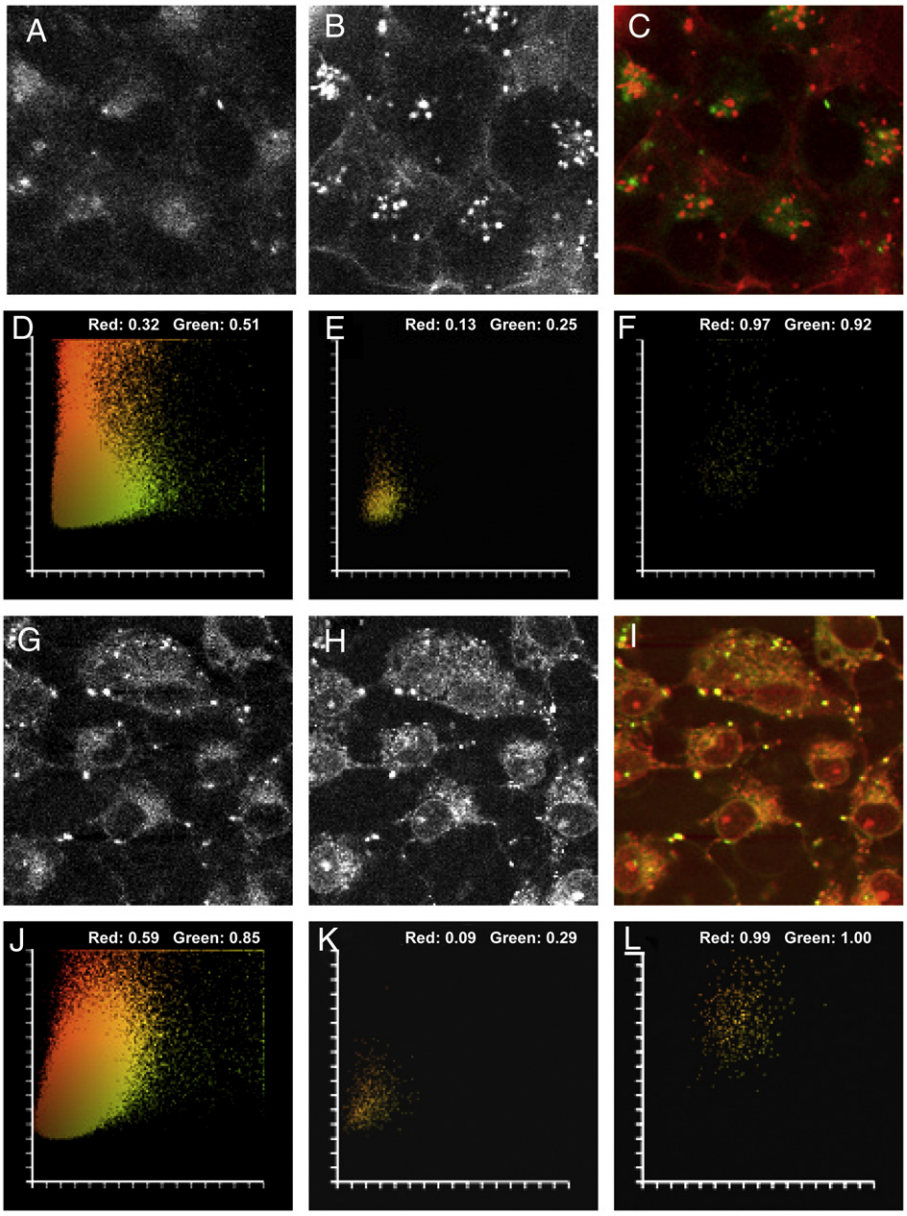

Fig. 6. Colocalization of TR-ACBP and DChol in membrane-bound vesicles/organelles versus cytosol of COS-7 cells. TR-ACBP and DChol were coincubated with cells in the presence of serum ± Pep-1 at 37 °C (see Materials and methods) and simultaneous images of the two fluorescent markers were acquired at short (10 min) or long (90 min) time periods after delivery starting point. (A1) DChol image at 10 min of serum (no Pep-1) incubation. (A2) TR-ACBP in same cells as in A1. (A3) Overlay of DChol (green) and TR-ACBP (red) at 10 min of serum (no Pep-1) incubation. (D) Fluorograph of red/green pixel colocalization when the entire area shown in panel A was selected for analysis. (E) Fluorograph of red/green pixel colocalization of a small area which was selected within cytosol (diffuse pattern of fluorescent markers inside cells). (F) Fluorograph of red/green pixel colocalization of a small area which was selected within vesicle/plasma membranes. (G–I) as in (A–C) respectively except that images were taken of cells which were incubated with DChol and TR-ACBP in serum plus Pep-1. (J– L) as in (D–F) respectively, except that images were taken of cells which were incubated with DChol and TR-ACBP in serum plus Pep-1.

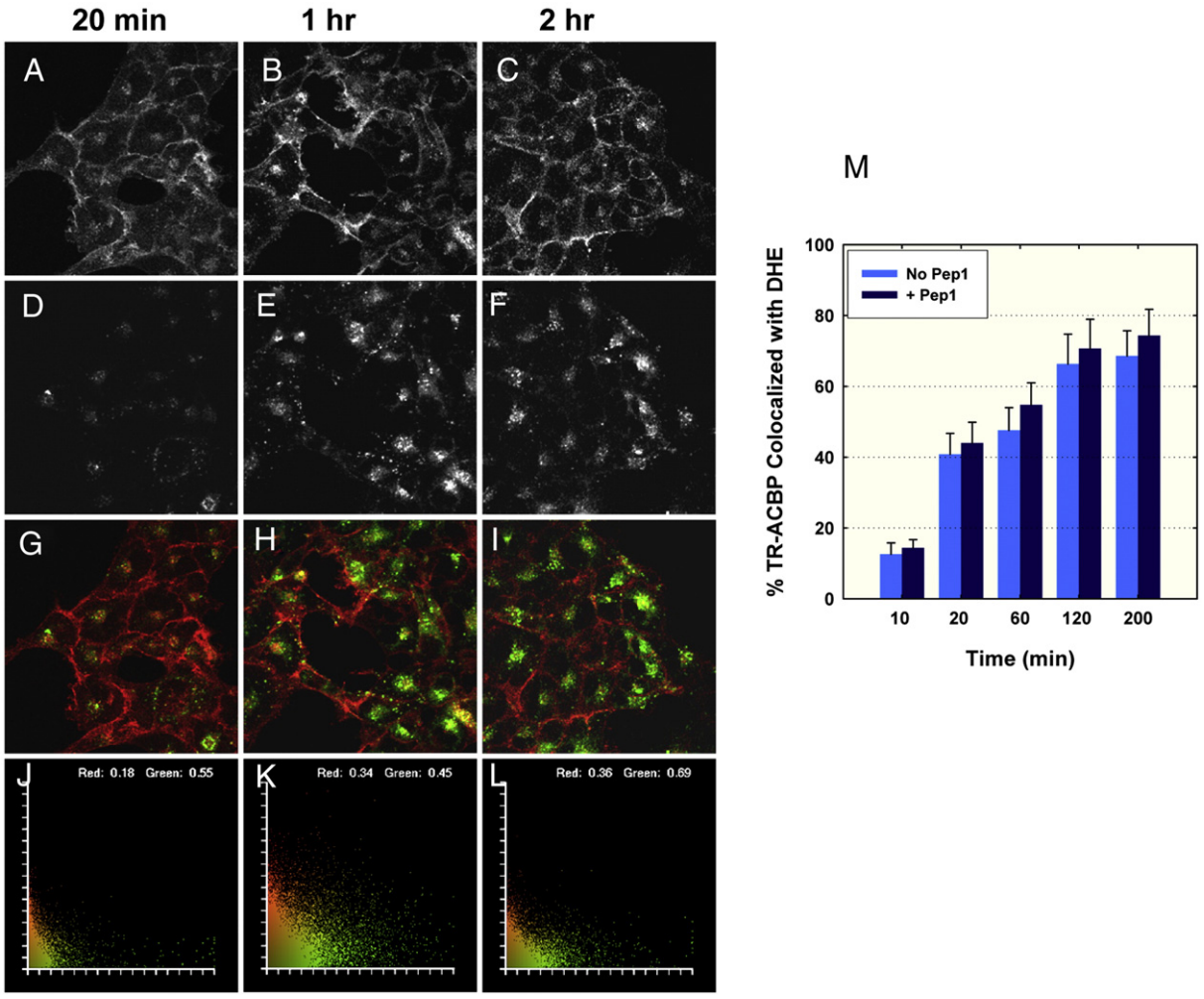

Fig. 7. DHE/TR-ACBP confocal colocalization monitored for TR-ACBP uptake into live COS-7 cells labeled with DHE/LUVs. (A–C) DHE fluorescence images in cells at different time points after addition of TR-ACBP. (D–F) TR-ACBP fluorescence images in same cells as shown in panels A-C. (G–I) TR-ACBP/DHE overlay images; TR-ACBP is shown in green, and DHE in red. (J–L) Fluorographs corresponding to each colocalization image shown above, respectively. (M) Bar plot of TR-ACBP percentage which was colocalized with DHE in the absence and presence of Pep-1, versus time.

membrane, while TR-ACBP (Fig. 4C2) was distributed in fewer, less intense, but more diffusely distributed small punctuate regions throughout the cell interior. In both cases neither marker appeared within the nuclei. At longer incubation time (1–2 h) the Alexa488-transferrin was distributed primarily in bright punctuate regions in the perinuclear area (Fig. 4D1) while TR-ACBP appeared not only as punctuate regions within the cell interior, but also in the nuclei (Fig. 4D2). Superposition of the images (Fig. 4C3), and even more so display of only colocalized pixels (Fig. 4C4), showed at short incubation time (10–30 min) the TR-ACBP was somewhat colocalized with the clathrin endocytosis pathway marker primarily in the perinuclear area and more diffusely in the cytoplasm. At longer incubation times (1–2 h), superposition (Fig. 4D3) and display of only colocalized pixels (Fig. 4D4) showed high intensity of colocalized TR-ACBP with Alexa488 dextran primarily in the perinuclear region and in larger punctuate structures within the cytoplasm. However, both at short and long incubation times, the intensity of TR-ACBP colocalization with the clathrin pathway marker (Fig. 4C4 and D4) was much less than that observed with the macropinocytosis marker (Fig. 4A4 and B4). Taken together these data suggest that TR-ACBP was internalized by both endocytic pathways, with the extent of macropinocytic uptake being more prevalent than that mediated by the clathrin endocytic pathway. Interestingly, TR-ACBP was taken up into COS7 cells in the absence of a cell penetrating peptide like Pep-1, albeit 2.4-fold less efficiently (see below). Uptake in the absence of Pep-1 was not due to TR labeling or the presence of the his tag in TR-his-ACBP. Control experiments showed that native ACBP (with no His or any other tag) also entered cells even in the absence of Pep-1.

3.5. Colocalization of Texas Red-ACBP with DChol in COS-7 cells preincubated with DChol in serum containing medium: effect of Pep-1

While the above studies indicate that cells can take up TR-ACBP by endocytic pathways, they do not provide insight as to the relative quantity of TR-ACBP that may enter the cytoplasm vs that retained in membranous structures, or if either process is facilitated by CPPs such as Pep-1. Therefore, the effect of Pep-1 on TR-ACBP uptake into COS-7 cells and colocalization with serum-delivered DChol was studied by incubating COS-7 cells with TR-ACBP (or TR-ACBP complexed with Pep-1) and DChol in serum-free (or serum-containing DMEM medium), followed by LSCM. In the absence of serum, no DChol was colocalized with TR-ACBP (yellow) inside the cells, regardless of the absence or presence of Pep-1 (Fig. 5A and B). Although a few yellow colocalized pixels were detected at the cell surface plasma membranes, quantitative analysis of multiple pixel fluorograms showed very little colocalization (3%) when cells were incubated with serum-free medium (Fig. 5B, left bar). In contrast, serum in the medium significantly facilitated DChol uptake: 12 ± 1.8 a.u/cell at 30 min, 19 ± 2.2 a.u./cell at 60 min, and 33 ± 4.3 a.u./cell at 2 h after addition of serum to cells in the presence of DChol in DMEM

culture medium. Furthermore, incubating cells with DChol in serum-containing medium (30 min, 120 min) resulted in increased appearance of colocalized TR-ACBP/DChol pixels inside cells, in a bright punctuate pattern, especially in the perinuclear area (Fig. 5A, top row). In the presence of serum, TR-ACBP was increasingly colocalized with DChol to a maximum near 40% (Fig. 5B). Concomitantly, the quantity of TR-ACBP not colocalized with DChol in vesicles/membranous structures was about 50–60% (Fig. 5C).

Pep-1 facilitated the uptake of TR-ACBP by COS-7 cells. Quantitative analysis of colocalization images (Fig. 5A, bottom row vs top row) indicated that Pep-1 increased TR-ACBP uptake such that 2.4 fold more TR-ACBP per cell was detected in the presence of Pep1/serum as compared to serum alone. Pep-1 increased the extent of colocalized TR-ACBP/DChol (yellow) pixels in both the cell interior and at the plasma membrane, especially in cells incubated with DChol in serum-containing medium (Fig. 5A, bottom row vs top row). TR-ACBP/DChol colocalization was increased in the absence of serum (6% vs 3%) and even more in the presence of serum—reaching a maximum of nearly 75% vs 35% (Fig. 5B). However, nearly 25% of TR-ACBP was not colocalized with DChol even at the longest incubation time examined (Fig. 5C).

To further determine where inside cells (cultured with DChol in serum containing medium) the TR-ACBP was colocalized with DChol, very small areas displaying the presence of DChol (Fig. 6A) and either high intensity, punctuate distributed TR-ACBP (vesicles/membranes, Fig. 6B) or diffuse non-punctate TR-ACBP intensity (cytosol, Fig. 6B) were selected for colocalization analysis. Superposition of DChol (Fig. 6A) and TR-ACBP (Fig. 6B) yielded a combined image (Fig. 6C) showing significant yellow/orange colocalized pixels with highest intensities in punctuate structures at the perinuclear regions of the cells and low intensities diffuse in the cytoplasm. Fluorographs of different areas selected from the latter image are shown (Fig. 6D–F) as follows: The fluorograph in Fig. 6D illustrates the distribution and colocalization coefficients when the entire area of the overlay image was selected. Fig. 6E and F exhibit the distribution and colocalization coefficients for small areas which were selected within cytosol (diffuse) or vesicles (compact), respectively. The latter graphs suggested that in the more diffuse areas (cytosol) only 13% of TR-ACBP was co-distributed with DChol, while the more punctuate and intense areas (vesicles, membranes) as much as 97% of TR-ACBP was colocalized with DChol. Incubation of cells with Pep-1/TR-ACBP complex in serum-containing medium had no effect on the degree of colocalization with DChol in the corresponding respective regions within the cell (Fig. 6G–L).

Taken together, these results indicate that: (i) serum facilitated TR-ACBP uptake regardless of the presence of Pep-1; (ii) in the presence of serum Pep-1 modestly increased TR-ACBP uptake 2.4-fold; (iii) Pep-1 increased the proportion of TR-colocalized with DChol in membranous structures at intermediate (30–90 min) incubation times—consistent with increased endocytic uptake; and (iv) Pep-1 did not significantly alter the proportion of TR-ACBP free in the cytoplasm (i.e. not colocalized with DChol-containing membranous structures) at longer incubation times.

3.6. Colocalization of TR-ACBP with dehyroergosterol (DHE) incorporated into COS-7 cells in the form of DHE/POPC LUVs

Because DChol is a synthetic, fluorescent sterol with a dansyl side group not occurring in nature, the possibility that the high degree of TR-ACBP codistribution with DChol on uptake into COS-7 cells might be specific to this fluorescent sterol rather than endogenous native sterol (e.g. cholesterol) was considered. Although cholesterol is non-fluorescent, this possibility was tested by examining the uptake and

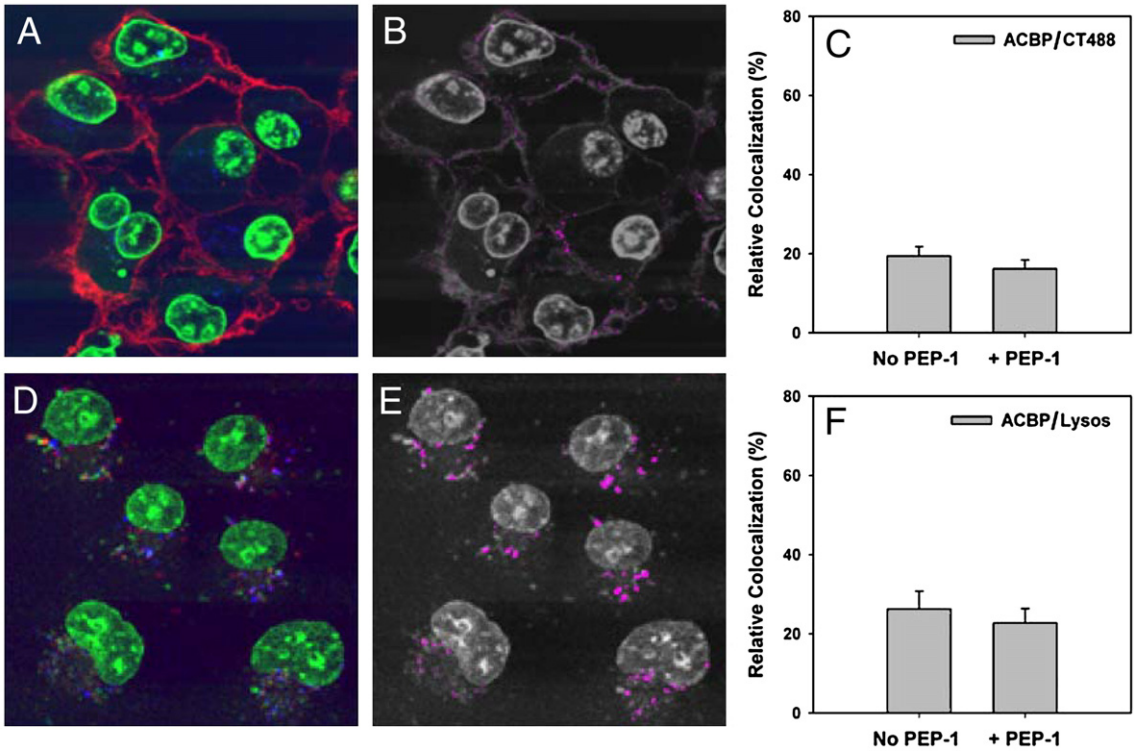

Fig. 8. Colocalization of Cy5-ACBP with plasma membrane lipid rafts and lysosomes in live cells. COS-7 cells were first treated with Cy5-ACBP in the absence (not shown) or presence of Pep-1 at 37 °C for 30 min, then labeled with Hoechst nuclear marker, and for either plasma membrane GM1-lipid rafts with Alexa Fluor488-cholera toxin B (at 4 °C, for 20 min), or for lysosomes with LysoTracker dye (at 37 °C for 30 min), as described in Materials and methods. (A) Overlay of Cy5-ACBP (blue), lipid raft marker (Alexa488-cholera toxin B, red) and nuclear Hoechst dye (green) images. (B) Only colocalized red and blue pixels in panel A were selected and shown in magenta. (C) Bar graph of percent colocalization of Cy5-ACBP with cholera toxin in COS-7 cells. (D) Overlay of Cy5-ACBP (blue), lysosome marker (Lysotracker, red) and nuclear marker (green) images. (E) Colocalized pixels of Cy5-ACBP and lysosome markers were selected and shown in magenta. (F) Bar graph of percent colocalization of Cy5-ACBP and lysosome marker in cells treated with or without Pep-1.

colocalization of TR-ACBP with the naturally-occurring fluorescent sterol dehydroergosterol (DHE). DHE exhibits high structural and functional similarity to cholesterol and codistributes with cholesterol in all membranes of the cell heretofore examined rev. in [16–20]. DHE has proven useful to image intracellular cholesterol trafficking by two-photon laser scanning confocal microscopy [30,32,33].

COS-7 cells were labeled with DHE by preincubation with DHE/POPC LUVs prior to incubation with TR-ACBP or Pep1/TR-ACBP as described in Materials and methods. With increasing incubation time DHE and TR-ACBP were taken up and distributed not only at the plasma membrane but also throughout the cell as shown for DHE (Fig. 7A–C) and TR-ACBP (Fig. 7D–F). Merged MPLSM images of TR-ACBP (green in Fig. 7G–I) and DHE (red in Fig. 7G–I) showed that, at early time points little TR-ACBP appeared inside the cells, but was instead distributed primarily at the plasma membrane (Fig. 7G). At longer time points TR-ACBP was increasingly colocalized with DHE at the plasma membrane and within cells as orange/yellow areas and also some in the perinuclear region. Quantitative analysis of multiple colocalized images showed that TR-ACBP/DHE colocalization coefficients were low, near 15% at early time points, but increased at longer times to plateau near 75% colocalization (Fig. 7J). Interestingly, the highest labeling of cells by TR-ACBP was observed within an area next to nucleus, corresponding to Golgi complex, which was also labeled by DHE. It has been previously demonstrated that DHE colocalized with BODIPY-C5-ceramide (Golgi marker) in another cell type, namely L-cells [32]. The data presented herein showed that DHE decorated COS-7 cells within similar areas close to nuclei and TR-ACBP codistributed with DHE in this region. Even if DHE was delivered by LUVs and 16 h incubation with serum before addition of TR-ACBP ± Pep-1, the Pep-1 had no significant effect on the TR-ACBP colocalization with DHE (Fig. 7M). These data were consistent with Pep-1 not affecting the proportion of DHE-containing membrane/organelle associated vs cytosolic TR-ACBP—confirming results obtained with DChol.

3.7. Intracellular targeting of fluorescent-labeled ACBP in live cells

We further examined the types of intracellular fluorescent sterol-containing organelles/membrane structures which were targeted by TR-ACBP when it was delivered to cells by serum in the absence and presence of Pep-1. Since most vital dye organelle markers emitted in the same region as Texas Red, ACBP was labeled with Cy5 instead of Texas Red. Similarly as for TR-labeling, Cy5-labeling did not or only slightly altered ACBP structural and functional features (data not shown). Therefore, COS-7 cells were first incubated with Cy5-ACBP in the absence or presence of Pep-1 for 1 h and then labeled with fluorescent vital dye markers for specific membrane-bound organelles (plasma membrane, lysosomes, endoplasmic reticulum, mitochondria) as described under Materials and methods. The nuclear marker (Hoechst 33342) and the plasma membrane cholesterol-rich microdomain marker, Alexa Fluor 488-cholera toxin subunit B, did not overlap significantly with other intracellular organelle markers examined (endoplasmic reticulum, mitochondria, lysosomes, Golgi). However, due to the relative abundance of intracellular organelle markers as well as the optical resolution of LSCM in the z-axis, there was ~10–15% overlap in distributions of the other intracellular organelle markers (endoplasmic reticulum, mitochondria, lysosomes, Golgi) with each other. Due to this overlap in organelle distributions, the colocalization percentages obtained for the latter dyes represented a relative colocalization of Cy5-ACBP with the lysosomal, mitochondrial, endoplasmic reticulum, and Golgi markers.

To determine the distribution of Cy5-ACBP to plasma membrane cholesterol-rich microdomains in living cells, the Cy5-ACBP was

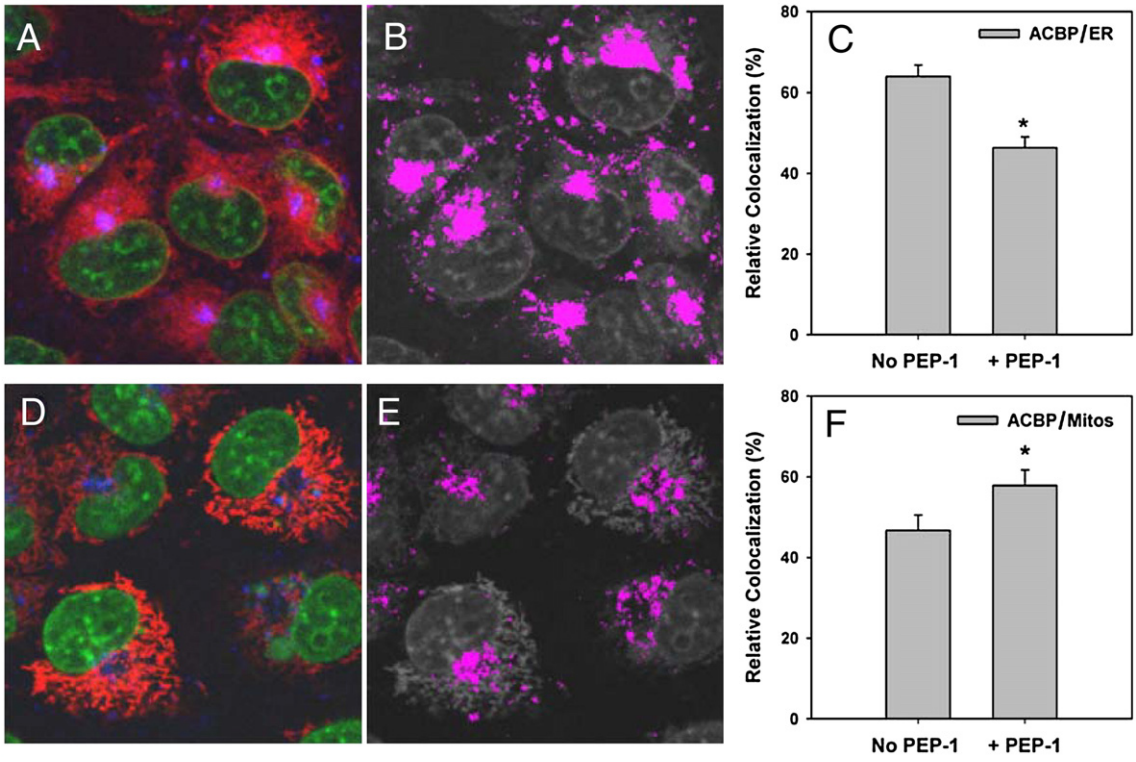

Fig. 9. Colocalization of Cy5-ACBP with endoplasmic reticulum (ER) and mitochondrial markers in live cells. COS-7 cells were first treated Cy5-ACBP in the absence (not shown) or presence of Pep-1 in serum (for 30 min at 37 °C), then labeled with nuclear marker and either ER or mitochondrial markers (for additional 30 min at 37 °C, as described in Materials and methods). (A) Overlay of Cy5-ACBP (blue), nuclear marker (green) and ER marker (red) images. (B) Colocalized pixels of Cy5-ACBP (blue) and ER (red) were selected and shown in magenta. (C) Bar graph of percent colocalization of Cy5-ACBP and ER marker in cells which were treated or not with Pep-1. (D) Overlay of Cy5-ACBP (blue), nuclei (green) and mitochondrial marker (red) images in cells (treated with Pep-1). (E) Colocalized pixels of Cy5-ACBP (blue) and mitochondrial marker (red) were selected and shown in magenta. (F) Bar graph of percent colocalization of Cy5-ACBP and mitochondrial marker in cells in the absence or presence of Pep-1.

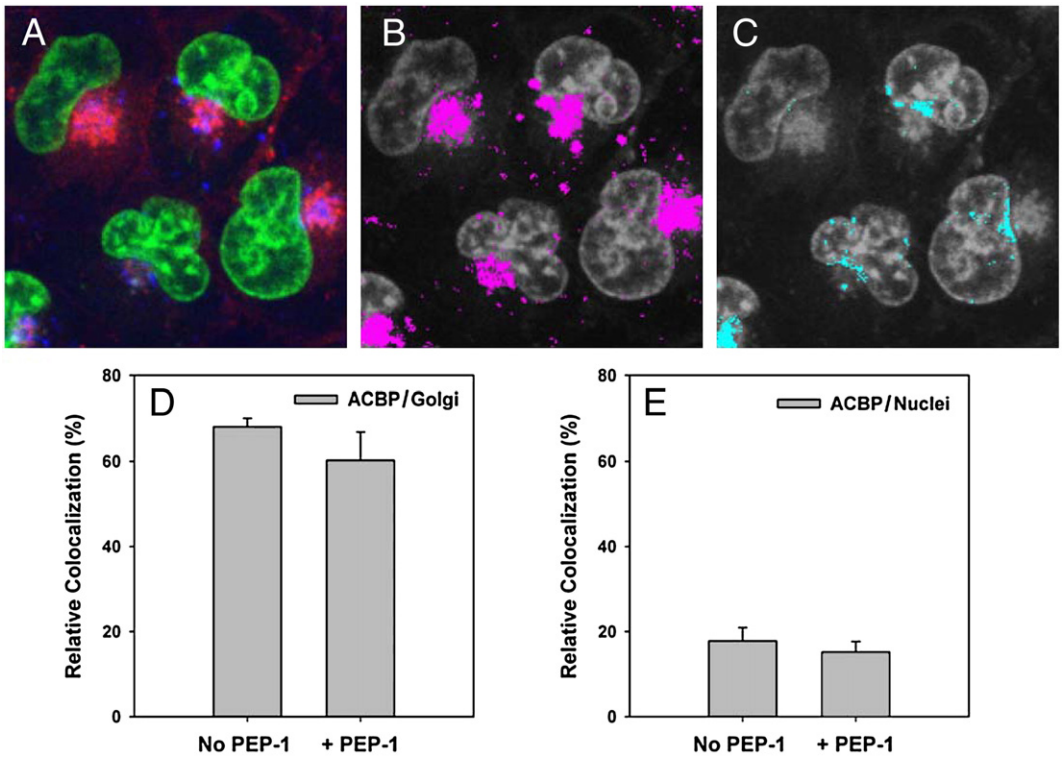

Fig. 10. Colocalization of Cy5-ACBP with Golgi and nuclear markers in live cells. COS-7 cells were first treated with Cy5-ACBP in the absence (not shown) and presence of Pep-1 (30 min at s37 °C), then labeled with nuclear marker Hoechst 33342 and Golgi complex marker, NBD-C6-ceramide (additional 30 min at 37 °C, see Materials and methods). (A) Overlay of Cy5-ACBP (blue), Golgi marker (red) and nuclear marker (green) in cells in the presence of Pep-1. (B) Colocalized pixels of Cy5-ACBP (blue in panel A) and Golgi marker (red in panel A) were selected and shown here in magenta. (C) Colocalized pixels of Cy5-ACBP (blue in panel A) and nuclear marker (green in panel A) were selected and shown here in turquoise. (D) Bar graph of percent colocalization of Cy5-ACBP with Golgi complex in cells in the absence and presence of Pep-1. (E) Bar graph of percent colocalization of Cy5-ACBP and nuclear marker in cells in the absence and presence of Pep-1.

colocalized with Alexa Fluor 488-cholera toxin-B (CTB) which binds with high affinity to ganglioside GM1 in plasma membrane cholesterol-rich microdomains [37]. COS-7 cells were first pre-incubated with Cy5-ACBP in the absence or presence of Pep-1 for 1 h at 37 °C, and then labeled for GM1 with Alexa Fluor-CTB at 4 °C. As shown by a representative overlay image of Cy5-ACBP (blue) and Alexa Fluor 488-CTB cholesterol-rich microdomain marker (red), CTB was located primarily at the plasma membrane (Fig. 8A) while ACBP was mostly inside cells and only rarely in proximity with CTB-labeled lipid rafts. When only colocalized pixels of Cy5-ACBP and Alexa Fluor 488-CTB were shown (Fig. 8B, pink), Cy5-ACBP at the plasma membrane appeared colocalized with cholesterol-rich microdomains at the plasma membrane, exhibiting a discontinuous clustered distribution therein. Calculated colocalization coefficients estimated ~18% of total fluorescent Cy5-ACBP colocalized with CT-B-488 cholesterol-rich microdomain marker (Fig. 8C). The presence of Pep-1 during incubation at 4 °C with Cy5-ACBP did not alter the extent (not shown) or codistribution of Cy5-ACBP to plasma membrane cholesterol-rich microdomains (Fig. 8C). These data suggest that Cy5-ACBP is more associated with cholesterol-rich microdomains at the plasma membrane than with endocytosed cholesterol-rich microdomains within the cell.

To show if Cy5-ACBP was also endocytosed via the lysosomal pathway, co-distribution with LysoTracker was examined. An overlay of respective images (Fig. 8D) showed lysosomal marker (red) primarily in random punctuate distribution mostly separate from Cy5-ACBP (blue). However, display of only colocalized pixels (Fig. 8E, pink) and quantitative analysis of correlation coefficients (Fig. 8F) indicated that ~24% of total Cy5-ACBP was colocalized with LysoTracker, slightly higher than the ~10–15% basal overlap of the two other organellar markers (endoplasmic reticulum and mitochondria shown below). Pep-1 did not affect co-distribution of Cy5-ACBP with lysosomes (Fig. 8F). Thus, the majority (i.e. other than ~9–14% over basal overlap) of Cy5-ACBP was not colocalized with lysosomes, consistent with ACBP primarily entering cells independently of the endocytic/lysosomal pathway.

Colocalization of Cy5-ACBP with endoplasmic reticulum (Fig. 9A–C) and mitochondrial (Fig. 9D–F) was significantly higher than basal. Superposition of Cy5-ACBP (blue) with endoplasmic reticulum or mitochondrial markers (red) demonstrated very different distribution patterns. The endoplasmic reticulum marker was more diffusely distributed within cytoplasm and exhibited thinner and more numerous fine, net-like tubules, very heavily distributed in perinuclear regions of the cells (Fig. 9A). In contrast, the mitochondrial marker was distributed in a more reticular, branched and confined to well-defined tubular form pattern (Fig. 9D). The endoplasmic reticulum and mitochondria markers were widely distributed throughout cytoplasm, resulting in considerable overlap of endoplasmic reticular and mitochondria markers (data not shown). Colocalized pixels of Cy5-ACBP with endoplasmic reticular marker (Fig. 9B) and mitochondrial marker (Fig. 9E), respectively, indicate that a larger number of Cy5-ACBP pixels colocalized with endoplasmic reticulum, especially in the perinuclear region, than with mitochondrial marker. Quantitative analysis indicated that ~63% of Cy5-ACBP was colocalized with ER (Fig. 9C), while ~46% colocalized with mitochondria (Fig. 9F). Pep-1 altered this distribution, significantly decreasing colocalization of Cy5-ACBP with endoplasmic reticulum marker (63% vs 45%) while concomitantly increasing codistribution with mitochondrial marker (46% vs 58%).

Colocalization images and analysis of ACBP with Golgi complex and nuclear markers showed the highest colocalization with Golgi and significantly less colocalization with nuclei. Superposition of Cy5-ACBP (blue) with Golgi (red) and nuclear (green) markers showed colocalized pixels mainly with Golgi in the perinuclear area (Fig. 10A). Display of colocalized pixels of Cy5-ACBP with Golgi (Fig. 10B, pink)

and nuclei (Fig. 10C, blue-green) demonstrate strong colocalization of Cy5-ACBP with Golgi, and a smaller but significant overlap of Cy5-ACBP with nuclei, especially near the nuclear envelope. Quantitative analysis showed ~70% of Cy5-ACBP colocalization with Golgi (Fig. 10D), but due to 10–15% overlap in distributions of Golgi, endoplasmic reticulum, and mitochondrial markers, the actual colocalization is near 55–60%. Finally, quantitative analysis showed ~18% of TR-ACBP colocalized with nuclei (Fig. 10E). Pep-1 had no effect on the relative distribution of TR-ACBP to either Golgi or nuclei.

In summary, colocalization of Cy5-ACBP with vital dye markers of intracellular organelles in living cells indicated that ACBP was associated with the intracellular membranous organelles in the following relative order: Golgi ≥ endoplasmic reticulum > mitochondria > lysosomes. Lesser amounts of Cy5-ACBP were also detected colocalized with cholesterol-rich microdomains of the plasma membrane, and within nuclei.

3.8. Intracellular distribution of endogenous ACBP in fixed cells: indirect immunofluorescence LSLCM

To test whether ACBP subcellular distribution determined by using TR-ACBP or Cy5-ACBP and vital dye markers reflected that of endogenous ACBP, intracellular distribution of endogenous ACBP was examined by immunofluorescence colocalization in fixed T-7 rat hepatoma cells. These cells were chosen because, unlike COS-7 cells, the hepatoma cells express high levels of endogenous ACBP. Hepatoma cells were fixed and double immunolabeled as described under Materials and methods. ACBP was colocalized with cholera toxin B (GM1 marker in plasma membrane cholesterol-rich microdomains), wheat germ agglutinin (WGA, Golgi marker), or cathepsin D (lysosome marker) (Fig. 11). Endogenous ACBP was distributed throughout the cells, with highest density in the perinuclear cytoplasm and lower but distinct distribution within nuclei and at the plasma membrane (Fig. 11A). Cholera toxin B decorated GM1 in bright patches of cholesterol-rich microdomains at the plasma membrane (Fig. 11B). The overlay of ACBP (red) and cholera toxin B (green) images in T-7 hepatoma cells (Fig. 11C) suggested significant colocalization of ACBP and GM1-rich cholesterol-rich microdomains in these cells. A computerized plot of only colocalized pixels of ACBP and cholera toxin B (Fig. 11D, yellow) confirmed that ACBP was codistributed with GM1 in cholesterol-rich microdomains at the plasma membrane. Panel D inset shows a 2.5 fold magnification of a plasma membrane region where ACBP and cholera toxin marker were colocalized in a clustered, non-random manner.

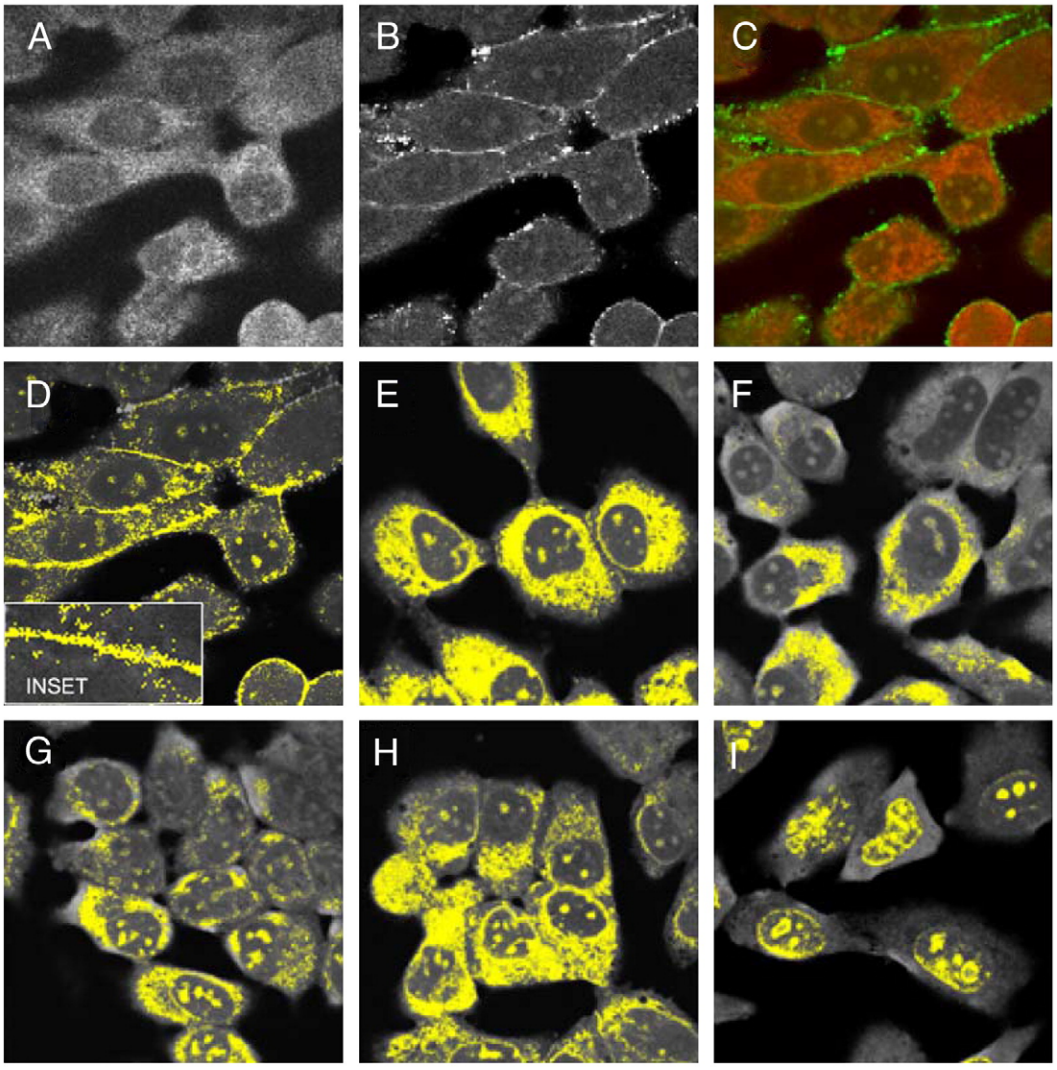

Fig. 11. Colocalization of ACBP with lipid raft, Golgi, lysosome, mitochondria, ER, and nuclear markers in T-7 rat hepatoma cells by indirect immunofluorescence confocal microscopy of fixed cells. (A) ACBP fluorescence image. (B) Cholera toxin B (GM1-lipid rafts) fluorescence image. (C) Overlay of ACBP (red) and cholera toxin B (green) images. (D) Colocalized pixels in panel C were selected and shown in yellow. Inset: magnification of colocalized pixels along a portion of plasma membrane. (E) Colocalization of ACBP with Golgi marker (WGA-FITC). (F) ACBP with lysosomes (cathepsin). (G) ACBP with mitochondria (HSP70). (H) ACBP with endoplasmic reticulum (concanavalin A). (I) ACBP with nuclei (Hoechst 33342).

Endogenous ACBP was also colocalized with several other intracellular organelle markers: First, a computerized plot of only colocalized pixels of ACBP and Golgi complex marker (WGA, Golgi marker) showed that ACBP codistributed strongly with WGA near the nuclei (Fig. 11E, yellow). Second, ACBP colocalized less so with lysosomes, especially near the cell periphery. Display of only colocalized pixels of ACBP with lysosomes showed weak colocalization in some cells, while other cells exhibited modest colocalization in the most intensely stained regions (Fig. 11F, yellow). Third, display of only colocalized pixels showed that endogenous ACBP also colocalized with mitochondrial marker heat shock protein-70 (HSP70) to similar extent as lysosomes, but in a more reticular pattern distributed in the cytoplasm (Fig. 11G, yellow). Fourth, display of colocalized pixels of ACBP with the endoplasmic reticulum marker (concanavalin A, ConA) showed a high level of ACBP co-distribution in the perinuclear region showing partial similarity in pattern as ACBP/Golgi (Fig. 11H, yellow). Fifth, display of colocalized pixels of ACBP with nuclear DNA-binding dye (Hoechst 33342) showed that ACBP was distributed within nuclei, strongly at the nuclear envelope and in nuclear membrane invaginations as well as more diffusely within nuclei (Fig. 11I, yellow). While some ACBP pixels appeared colocalized with organelle markers in the nuclear region, this was not due to the presence of these markers within nuclei, but rather to LSCM resolution in the z-axis and cell thinning in response to dehydration during the fixation process — a problem much less associated with LSCM of living cells.

Quantitative estimations by colocalization coefficient analysis indicated that endogenous ACBP in fixed rat hepatoma cells was distributed with the above intracellular organelle markers in the following order: Golgi≥endoplasmic reticulum>mitochondria>lysosome. ACBP was also detected in cholesterol-rich microdomains of the plasma membrane and within nuclei. Thus, immunofluorescence LSCM examination and colocalization analysis of ACBP in a cell line with high endogenous ACBP expression paralleled the results obtained with Cy5- ACBP and vital dye organelle markers in live COS-7 cells.

4. Discussion

While most studies of CPP mediated protein transduction have focused on mechanism(s) of uptake into the cell, little is known regarding the relative amount of cargo protein that subsequently emerges free in the cytoplasm for distribution to appropriate intracellular targets similar to endogenous cargo protein. The current investigation presented for the first time the use of fluorescent sterols (DChol, DHE) as markers for determining the relative proportion of cargo protein free in cytosol/nucleoplasm vs associated with endocytic vesicles/organelle membranes. For these studies ACBP was chosen as a cargo protein because: (i) ACBP is a ubiquitous intracellular protein expressed in most tissues/cells; (ii) ACBP is soluble in the cytosol as well as associated with select membranes/organelles; (iii) ACBP is sufficiently small (10 kDa) to pass through nuclear pores to enter the nucleoplasm wherein it directly interacts with nuclear receptors [22,38]. Since endocytosed vesicles are too large to pass through nuclear pores, the appearance of ACBP in the nucleoplasm provides another measure of exit of exogenously added ACBP from endocytic vesicles. These studies yielded several new insights:

First, real-time laser scanning microscopy (LSCM, MPLSM) of fluorescent sterols (DChol, DHE) showed these sterols were distributed in plasma membranes, plasma membrane cholesterol-rich microdomains, endocytic vesicles, and intracellular organelles/membranes in living cells. The data showed DChol as a brightly-fluorescent, synthetic sterol readily visualized by LSCM both at the plasma membrane and intracellular membranes of living COS-7 cells. Similar findings were obtained with DHE (a low quantum yield, naturally-occurring fluorescent sterol readily visualized by MPLSM) in COS-7 cells — consistent with MPLSM imaging of DHE in L-cell fibroblasts [32,33]. The real-time imaging studies were also supported by the results of subcellular fractionation and chemical analysis which showed that: (i) DHE codistributes with cholesterol in plasma membranes of cultured (L-cell, MDCK) cells [39,40], significantly more with cholesterol-rich than –poor microdomains [41–44]; (ii) DHE codistributes with cholesterol in intracellular membranes such as mitochondria [39,45], endoplasmic reticulum [39], and lysosomes [46] of cultured L-cell fibroblasts. Finally, the membrane distributions of DChol and DHE reflected those of cholesterol which is present in all cellular membranes with the exception of the inner mitochondrial membrane (rev. in [16,17,20]. Thus, the fluorescent sterols provided a novel means for real-time imaging of spontaneous and CPP-mediated protein cargo transduction, exit from endocytic uptake, and intracellular redistribution within the cell.

Second, the fluorescent sterols were useful as markers of endocytic uptake pathways in living cells. DChol colocalized with plasma membrane specialized domains labeled by cholera toxin B which binds to GM1 ganglioside in cholesterol-rich microdmains suggesting uptake via GM 1 cholesterol-rich microdomain-related pathways. Even though GM1 was first reported to be located in caveolae, more recent reports indicate that GM1 can also be associated with cholesterol-rich microdomains in macropinocytosis compartments [47–49]. Cholesterol-rich microdomain-associated GM1 was selectively included into macropinosomes [49]. The intracellular uptake of cholesterol from serum (containing LDL, HDL) also occurs by endocytosis pathways including: i) LDL-receptor mediated endocytosis through clathrin-coated vesicles [50]; ii) HDL-receptor, SR-BI-mediated uptake/efflux at the caveolae level [51]; iii) receptor-independent uptake of LDL by fluid phase or macropinocytosis [52]. In the present study, DChol was shown to colocalize with markers for the clathrin-mediated endosomal/lysosomal pathway (Transferrin) and nearly twice as much with the macropinocytosis pathway (TR-dextran) — consistent with high codistribution of DChol with CT-B (marker for GM1 in cholesterol-rich microdomains). Thus, DChol was similar to naturally-fluorescent sterol DHE in that DChol was not highly associated with the clathrin-coated pit endocytic unless the sterol was crystalline in the medium [32,46].

Third, Pep-1 enhanced ACBP translocation into COS-7 cells by 2.4-fold via pathways similar to those employed for DChol uptake, i.e. mostly macropinocytosis and less so clathrin-mediated endocytosis. Pep-1 is known to enhance the rate of macropinocytosis of other types of cargo protein [53]. The enhancing effect of Pep-1 upon macropinocytosis-mediated uptake of TR-ACBP and colocalization with DChol was abolished when DChol was delivered to cells by methyl-β-cyclodextrin (data not shown). This finding was consistent with the reported ability of cyclodextrin to interfere with cholesterol in cholesterol-rich microdomains and to inhibit macropinocytosis [53].

Fourth, TR-ACBP was translocated into COS-7 cells even in the absence of Pep-1, albeit 2.4-fold less efficiently. This finding might be explained by at least two possibilities: (i) The presence of a CPP-like domain in ACBP itself. The amino acid sequence of mouse ACBP has several putative NLS (nuclear localization signals which are characteristic for CPPs) domains (e.g. LKKKYGI with three lysine residues grouped together at the C-end of the molecule; VKRLKT with two lysines and an arginine in close proximity), but these sequences do not contain hydrophobic residues to enforce interaction with phospholipid membranes. However, an additional basic and hydrophobic amino acid-rich domain (a.a. 50–65) comprised of LKGKAKWDSWNKLKGT contains 5 lysine (K) residues alternating with two tryptophans (W) which might resemble the structure of a CPP such as Pep-1. (ii) Serum components that facilitate macropinocytic uptake of plasma membrane bound ACBP. ACBP is known to bind to anionic phospholipid containing but not neutral charged phospholipid containing model membranes [54,55]. Serum contains fetuin/alpha2-HS glycoprotein which has been shown to increase the uptake of dextran by cells through macropinocytosis [56]. Interestingly, extraction of cholesterol from cellular plasma membranes inhibited macropinosomes by

disrupting cholesterol-rich microdomains and by negatively affecting actin organization and small GTP-ase Rac-1 activity, which were demonstrated to be involved in macropinosome formation [57]. Taken together these data suggested that the basic amino acid-rich domains in ACBP were insufficient to induce ACBP translocation into COS-7 cells, but together with serum components this uptake was facilitated even in the absence of CPP such as Pep-1.

Fifth, a significant portion TR-ACBP translocated into COS7 cells entered the cytoplasm. About 20–40% of TR-ACBP taken up was not colocalized with DChol containing vesicles/organelle membranes and appeared free in the cytosol/nucleoplasm. With regards to the membrane component, TR-ACBP taken up by endocytosis was distributed similarly as endogenous ACBP to Golgi≥endoplasmic reticulum>mitochondria>lysosome>plasma membrane cholesterol-rich microdomains, and nuclei. ACBP colocalization with endoplasmic reticulum of living cells was consistent with its role in facilitating transacylation steps in fatty acid esterification to cholesteryl esters and glycerophospholipid (phosphatidic acid) [58,59]. Likewise, ACBP colocalization with mitochondria of living cells suggested that ACBP may also enhance transfer of bound long chain fatty acyl CoA to carnitine palmitoyl transferase I (CPT1), the rate limiting enzyme in mitochondrial fatty acid oxidation, located at the outer mitochondrial membrane [60,61]. Consistent with this possibility, ACBP enhances the activity of CPT1 *in vitro* [60,61]. Finally, appearance of ACBP in nuclei of living cells was consistent with earlier fixed cell experiments detecting ACBP in nuclei and with studies showing that ACBP overexpression transactivates nuclear transcription factors such as HNF4α [22,62]. Finally, detection of TR-ACBP in nuclei and nucleoplasm of living cells provides an important control indicating that the TR-ACBP was released from endocytic vesicles for transport into the nucleoplasm. Pores in the nuclear envelope double membrane are sufficiently large to accommodate small proteins such as ACBP (10 kDa), but not endocytic vesicles (rev. in [21]).

Sixth, Pep-1 selectively altered the intracellular targeting/distribution of ACBP without altering the proportion that membrane associated vs cytosolic/nucleoplasmic. Since Pep-1 enhanced uptake of TR-ACBP by 2.4-fold, this was consistent with the majority of TR-ACBP exiting endocytic compartment(s). Further consistent with this finding was the fact that Pep-1 facilitated colocalization of ACBP with mitochondria, reduced colocalization with endoplasmic reticulum, but did not alter colocalization with plasma membrane cholesterol-rich microdomains, lysosomes, or nuclei. While the molecular basis for this observation remains to be resolved, it may relate to channeling of cargo protein taken up by different endocytic mechanisms.

In summary, the work presented herein showed for the first time that the fluorescent sterols (DChol, DHE) were useful markers for comparing the membrane/organelle vs soluble (cytosol, nucleoplasm) distributions of both exogenous translocated and endogenous proteins. While Pep-1 did not alter the relative proportions of membrane vs cytosol/nucleoplasm associated TR-ACBP, the translocation of TR-ACBP into living cells was modestly increased 2.4-fold. In addition, Pep-1 altered the intracellular targeting of exogenous-delivered (TR-ACBP) by shifting TR-ACBP distribution away from endoplasmic reticulum toward mitochondria.

Acknowledgments

This work was supported in part by the USPHS, NIH DK41402 (FS, ABK) and GM31651 (FS, ABK).

References

[1] B. Gupta, T.S. Levchenko, V.P. Torchilin, Intracellular delivery of large molecules and small particles by cell-penetrating proteins and peptides, Adv. Drug Deliv. Rev. 57 (2005) 637–651.
[2] S.T. Henriques, M.A. Castanho, Consequences of non-lytic membrane perturbation to the translocation of the cell penetrating peptide Pep-1 in lipidic vesicles, Biochemistry 43 (2004) 9716–9724.
[3] J.S. Wadia, S.F. Dowdy, Protein transduction technology, Curr. Opin. Biotechnol. 13 (2002) 52–56.
[4] S.T. Henriques, M.N. Melo, M.A. Castanho, How to address CPP and AMP translocation? Methods to detect and quantify peptide internalization in vitro and in vivo, Mol. Membr. Biol. 24 (2007) 173–184.
[5] R. Fischer, M. Fotin-Mleczek, H. Hufnagel, R. Brock, Break on through to the other side–biophysics and cell biology shed light on cell-penetrating peptides, ChemBioChem 6 (2005) 2126–2142.
[6] M.C. Morris, J. Depollier, J. Mery, F. Heitz, G. Divita, A peptide carrier for the delivery of biologically active proteins into mammalian cells, Nat. Biotechnol. 19 (2001) 1173–1176.
[7] P.E.G. Thoren, D. Persson, E.K. Esbjorner, M. Goksor, P. Lincoln, B. Norder, Membrane binding and translocation of cell-penetrating peptides, Biochemistry 43 (2004) 3471–3489.
[8] J.S. Wadia, S.F. Dowdy, Transmembrane delivery of protein and peptide drugs by TAT-mediated transduction in the treatment of cancer, Adv. Drug Deliv. Rev. 57 (2005) 579–596.
[9] S. Futaki, Membrane-permeable arginine-rich peptides and the translocation mechanisms, Adv. Drug Deliv. Rev. 57 (2005) 547–558.
[10] P.E.G. Thoren, D. Persson, P. Lincoln, B. Norden, Membrane destabilizing properties of cell-penetrating peptides, Biophys. Chem. 114 (2005) 169–179.
[11] K. Weller, S. Lauber, M. Lerch, A. Renaud, H.P. Merkle, O. Zerbe, Biophysical and biological studies of end-group-modified derivatives of Pep-1, Biochemistry 44 (2005) 15799–15811.
[12] S.T. Henriques, J. Costa, M.A. Castanho, Translocation of beta-galactosidase mediated by the cell penetrating peptide Pep-1 into lipid vesicles and human HeLa cells is driven by membrane electrostatic potential, Biochemistry 44 (2005) 10189–10198.
[13] S.T. Henriques, M.A. Castanho, Environmental factors that enhance the action of the cell penetrating peptide pep-1: a spectroscopic study using lipidic vesicles, Biochim. Biophys. Acta 1669 (2005) 75–86.
[14] I. Nakase, M. Niwa, T. Takeuchi, K. Sonomura, N. Kawabata, Y. Koike, M. Takehashi, S. Tanaka, K. Ueda, J.C. Simpson, A.T. Jones, Y. Sugiura, S. Futaki, Cellular uptake of arginine-rich peptides: roles for macropinocytosis and actin rearrangement, Molec. Ther. 10 (2004) 1011–1022.
[15] K.O. Orii, J.H. Grubb, C. Vogler, B. Levy, Y. Tan, K. Markova, B.L. Davidson, Q. Mao, T. Orii, N. Kondo, W.S. Sly, Defining the pathway for Tat-mediated delivery of beta-glucuronidase in cultured cells and MPS VII mice, Molec. Ther. 12 (2005) 345–352.
[16] F. Schroeder, J.R. Jefferson, A.B. Kier, J. Knittell, T.J. Scallen, W.G. Wood, I. Hapala, Membrane cholesterol dynamics: cholesterol domains and kinetic pools, Proc. Soc. Exp. Biol. Med. 196 (1991) 235–252.
[17] F. Schroeder, A.A. Frolov, E.J. Murphy, B.P. Atshaves, J.R. Jefferson, L. Pu, W.G. Wood, W. B. Foxworth, A.B. Kier, Recent advances in membrane cholesterol domain dynamics and intracellular cholesterol trafficking, Proc. Soc. Exp. Biol. Med. 213 (1996) 150–177.
[18] F. Schroeder, A. Frolov, J. Schoer, A. Gallegos, B.P. Atshaves, N.J. Stolowich, A.I. Scott, A.B. Kier, Intracellular sterol binding proteins, cholesterol transport and membrane domains, in: T.Y. Chang, D.A. Freeman (Eds.), Intracellular Cholesterol Trafficking, Kluwer Academic Publishers, Boston, 1998, pp. 213–234.
[19] F. Schroeder, A.M. Gallegos, B.P. Atshaves, S.M. Storey, A. McIntosh, A.D. Petrescu, H. Huang, O. Starodub, H. Chao, H. Yang, A. Frolov, A.B. Kier, Recent advances in membrane cholesterol microdomains: rafts, caveolae, and intracellular cholesterol trafficking, Exp. Biol. Med. 226 (2001) 873–890.
[20] F. Schroeder, B.P. Atshaves, A.M. Gallegos, A.L. McIntosh, J.C. Liu, A.B. Kier, H. Huang, J.M. Ball, Lipid rafts and caveolae organization. in: P.G. Frank, M.P. Lisanti (Eds.), Advances in Molecular and Cell Biology, vol. 36, Advances in Molecular and Cell Biology, Elsevier, Amsterdam, 2005, pp. 3–36.
[21] F. Schroeder, A.D. Petrescu, H. Huang, B.P. Atshaves, A.L. McIntosh, G.G. Martin, H.A. Hostetler, A. Vespa, K. Landrock, D. Landrock, H.R. Payne, A.B. Kier, Role of fatty acid binding proteins and long chain fatty acids in modulating nuclear receptors and gene transcription, Lipids 43 (2008) 1–17.
[22] A.D. Petrescu, H.R. Payne, A.L. Boedeker, H. Chao, R. Hertz, J. Bar-Tana, F. Schroeder, A.B. Kier, Physical and functional interaction of acyl CoA binding protein (ACBP) with hepatocyte nuclear factor-4alpha (HNF4alpha), J. Biol. Chem. 278 (2003) 51813–51824.
[23] A.D. Petrescu, R. Hertz, J. Bar-Tana, F. Schroeder, A.B. Kier, Ligand specificity and conformational dependence of the hepatic nuclear factor-4alpha (HNF-4a), J. Biol. Chem. 277 (2002) 23988–23999.
[24] A.D. Petrescu, H. Huang, H.A. Hostetler, F. Schroeder, A.B. Kier, Structural and functional characterization of a new recombinant histidine-tagged acyl CoA binding protein (ACBP) from mouse, Protein Exp. Purif. 58 (2008) 184–193.
[25] U.K. Laemmli, Cleavage of structural proteins during the assembly of the head of bacteriophage T4, Nature (London) 227 (1970) 680–685.
[26] B.B. Kragelund, J. Knudsen, F.M. Poulsen, Acyl-coenzyme A binding protein (ACBP), Biochim. Biophys. Acta 1441 (1999) 150–161.
[27] N. Sreerama, R.W. Woody, Structural composition of beta-I and beta-II proteins, Protein Sci. 12 (2003) 384–388.
[28] H.A. Hostetler, A.D. Petrescu, A.B. Kier, F. Schroeder, Peroxisome proliferator activated receptor alpha (PPARalpha) interacts with high affinity and is conformationally responsive to endogenous ligands, J. Biol. Chem. 280 (2005) 18667–18682.
[29] V. Wiegand, T.-Y. Chang, J.F. Strauss III, F. Fahrenholz, G. Gimpl, Transport of plasma membrane derived cholesterol and the function of Niemann-Pick C1 protein, FASEB J. 17 (2003) 782–784.
[30] A.L. McIntosh, B.P. Atshaves, H. Huang, A.M. Gallegos, A.B. Kier, F. Schroeder, Fluorescence techniques using dehydroergosterol to study cholesterol trafficking, Lipids (2008) doi:10.1007/s11745-008-3194-1.

[31] A. McIntosh, B.P. Atshaves, H. Huang, A.M. Gallegos, A.B. Kier, F. Schroeder, H. Xu, W. Zhang, S. Liu, Multiphoton laser scanning microscopy and spatial analysis of dehydroergosterol distributions on plasma membranes of living cells, in: T. McIntosh (Ed.), Lipid Rafts, Methods in Molecular Biology, Humana Press Inc., Totowa, N.J., 2007, pp. 85–105.
[32] A. McIntosh, A. Gallegos, B.P. Atshaves, S. Storey, D. Kannoju, F. Schroeder, Fluorescence and multiphoton imaging resolve unique structural forms of sterol in membranes of living cells, J. Biol. Chem. 278 (2003) 6384–6403.
[33] W. Zhang, A. McIntosh, H. Xu, D. Wu, T. Gruninger, B.P. Atshaves, J.C.S. Liu, F. Schroeder, Structural analysis of sterol distribution in the plasma membrane of living cells, Biochemistry 44 (2005) 2864–2984.
[34] H. Huang, B.P. Atshaves, A. Frolov, A.B. Kier, F. Schroeder, Acyl-coenzyme A binding protein expression alters liver fatty acyl coenzyme A metabolism, Biochemistry 44 (2005) 10282–10297.
[35] H. Huang, O. Starodub, A. McIntosh, B.P. Atshaves, G. Woldegiorgis, A.B. Kier, F. Schroeder, Liver fatty acid binding protein colocalizes with peroxisome proliferator receptor alpha and enhances ligand distribution to nuclei of living cells, Biochemistry 43 (2004) 2484–2500.
[36] N.J. Faergeman, J. Knudsen, Role of long-chain fatty acyl-CoA esters in the regulation of metabolism and in cell signalling, Biochem. J. 323 (1997) 1–12.
[37] A.T. Aman, S. Fraser, E.A. Merritt, C. Rodigherio, M. Kenny, M. Ahn, W.G.J. Hol, N.A. Williams, W.E. Lencer, T.R. Hirst, A mutant cholera toxin B submunit that binds GM1-ganglioside but lacks immunomodulatory or toxic activity, Proc. Natl. Acad. Sci. U. S. A. 98 (2001) 8536–8541.
[38] R.E. Gossett, A.A. Frolov, J.B. Roths, W.D. Behnke, A.B. Kier, F. Schroeder, Acyl Co A binding proteins: multiplicity and function, Lipids 31 (1996) 895–918.
[39] A. Frolov, J.K. Woodford, E.J. Murphy, J.T. Billheimer, F. Schroeder, Spontaneous and protein-mediated sterol transfer between intracellular membranes, J. Biol. Chem. 271 (1996) 16075–16083.
[40] A.M. Gallegos, B.P. Atshaves, S. Storey, A. McIntosh, A.D. Petrescu, F. Schroeder, Sterol carrier protein-2 expression alters plasma membrane lipid distribution and cholesterol dynamics, Biochemistry 40 (2001) 6493–6506.
[41] B.P. Atshaves, A. Gallegos, A.L. McIntosh, A.B. Kier, F. Schroeder, Sterol carrier protein-2 selectively alters lipid composition and cholesterol dynamics of caveolae/lipid raft vs non-raft domains in L-cell fibroblast plasma membranes, Biochemistry 42 (2003) 14583–14598.
[42] A.M. Gallegos, S.M. Storey, A.B. Kier, F. Schroeder, J.M. Ball, Stucture and cholesterol dynamics of caveolae/raft and nonraft plasma membrane domains, Biochem. 45 (2006) 12100–12116.
[43] A.M. Gallegos, A.L. McIntosh, A.B. Kier, F. Schroeder, Membrane domain distributions: Analysis of fluorescent sterol exchange kinetics, Curr. Anal. Chem. 4 (2008) 1–7.
[44] S.M. Storey, A.M. Gallegos, B.P. Atshaves, A.L. McIntosh, G.G. Martin, K. Landrock, A.B. Kier, J.A. Ball, F. Schroeder, Selective cholesterol dynamics between lipoproteins and caveolae/lipid rafts, Biochemistry 46 (2007) 13891–13906.
[45] A.M. Gallegos, J. Schoer, O. Starodub, A.B. Kier, J.T. Billheimer, F. Schroeder, A potential role for sterol carrier protein-2 in cholesterol transfer to mitochondria, Chem. Phys. Lipids 105 (2000) 9–29.
[46] J. Schoer, A. Gallegos, O. Starodub, A. Petrescu, J.B. Roths, A.B. Kier, F. Schroeder, Lysosomal membrane cholesterol dynamics: role of sterol carrier protein-2 gene products, Biochemistry 39 (2000) 7662–7677.
[47] R.D. Singh, V. Puri, J.T. Valiyaveettil, D.L. Marks, R. Bittman, R.E. Pagano, Selective caveolin-1 dependent endocytosis of glycosphingolipids, Mol. Biol. Cell 14 (2003) 3254–3265.
[48] B. Schneisder, C. Schuller, O. Utermoehlen, A. Haas, Lipid microdomain dependent macropinocytosis determines compartmentation of Afipia Felis, Traffic 8 (2007) 226–240.
[49] S. Kim, M. Watarai, S. Makino, T. Shirahata, Membrane sorting during swimming internalizaiton of Brucella is required for phagosome trafficking decisioin.ipid microdomain dependent macropinocytosis determines compartmentation of Afipia Felis, Microb. Pathol. 33 (2002) 225–237.
[50] E. Turpin, M. Bomsel, C. de Paillerets, A. Alfsen, Specific lipid protein interactions characterize three populations of clathrin coated vesicles involved in the LDL receptor traffic, CR Acad. Sci. III 319 (1996) 493–503.
[51] G.A. Graf, P.M. Connell, D.R. van der Westhuyzen, E.J. Smart, The class B, Type 1 scavenger receptor promotes the selective uptake of high density lipoprotein cholesterol ethers into caveolae, J. Biol. Chem. 274 (1999) 12034–12048.
[52] B. Zhao, Y. Li, S.W. Waldo, N.L. Jones, M. Mori, H.S. Kruth, Constitutive receptor independent LDL uptake and cholesterol accumulation by macrophages differentiated from human monocytes with M-CSF, J. Biol. Chem. 281 (2006) 15757–15762.
[53] J.S. Wadia, R.V. Stan, S.F. Dowdy, Transducible TAT HA fusogenic peptide enhnaces escape of TAT-fusion proteins after lipid raft macropinocytosis, Nat. Med. 10 (2004) 310–315.
[54] H. Chao, G. Martin, W.K. Russell, S.D. Waghela, D.H. Russell, F. Schroeder, A.B. Kier, Membrane charge and curvature determine interaction with acyl CoA binding protein (ACBP) and fatty acyl CoA targeting, Biochemistry 41 (2002) 10540–10553.
[55] A. Sharanov, R. Bandichhor, K. Burgess, A.D. Petrescu, F. Schroeder, A.B. Kier, and R. Hochstrasser, Single molecule tracks of a dynamicallly associated external label provide fluid properties of free-standing giant unilamellar vesicle membranes and supported bilayers, Langmuir in press 11–5–07 (2007).
[56] H.P. Jersmann, I. Dransfield, S.P. Hart, Fetuin/alpha2-HS glycoproetin enhances phagocytosis of apoptotic cells and macropinocytosis by human macrophages, Clin. Sci. (London) 105 (2003) 203–208.
[57] S. Grimmer, B. van Deurs, K. Sandvig, Membrane ruffling and macropinocytosis in A431 cells require cholesterol, J. Cell. Sci. 115 (2002) 2953–2962.
[58] C.A. Jolly, D.A. Wilton, F. Schroeder, Microsomal fatty acyl CoA transacylation and hydrolysis: fatty acyl CoA species dependent modulation by liver fatty acyl CoA binding proteins, Biochim. Biophys. Acta 1483 (2000) 185–197.
[59] H. Chao, M. Zhou, A. McIntosh, F. Schroeder, A.B. Kier, Acyl CoA binding protein and cholesterol differentially alter fatty acyl CoA utilization by microsomal acyl CoA: cholesterol transferase, J. Lipid Res. 44 (2003) 72–83.
[60] A.K.M.J. Bhuiyan, S.V. Pande, Carnitine palmitoyltransferase activities: effects of serum albumin, acyl-CoA binding protein and fatty acid binding protein, Mol. Cell. Biochem. 139 (1994) 109–116.
[61] K.A.H. Abo-Hashema, M.H. Cake, M.A. Lukas, J. Knudsen, The interaction of acyl CoA with acyl CoA binding protein and carnitine palmitoyltransferase I, Int. J. Biochem. Cell Biol. 33 (2001) 807–815.
[62] T. Hellendie, M. Antonius, R.V. Sorensen, A.V. Hertzel, D.A. Bernlohr, S. Kolvraa, K. Kristiansen, S. Mandrup, Lipid binding proteins modulate ligand-dependent trans-activation by peroxisome proliferator-activated receptors and localize to the nucleus as well as the cytoplasm, J. Lipid Res. 41 (2000) 1740–1751.